Master Thesis

2005

Decay of correlations in squash-shaped billiards

Orsolya Rappné Pogány

Supervisor: András Vetier Dr.
Budapest University of Technology and Economics
Department of Stochastics

Consultants: Imre Péter Tóth
Péter Bálint Dr.

Contents

1 Introduction and historical overview

A billiard is a dynamical system where a point particle moves freely (neglecting friction) at unit speed in a domain Q (the "table") and bounces off its boundary ∂Q (the "wall") by the classical rule "the angle of incidence with the normal of the curve equals to the angle of reflection" (see Figure 1). The domain Q is finite, and its boundary may consist of convex or concave walls or bumpers. We assume that $Q \subset \mathbb{R}^2$ or $\mathbb{T}^2$, and that the boundary is a finite union of smooth curves.

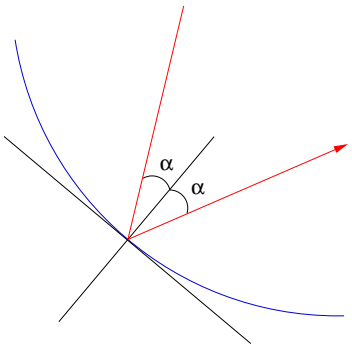

Figure 1: *The angles of incidence and reflection*

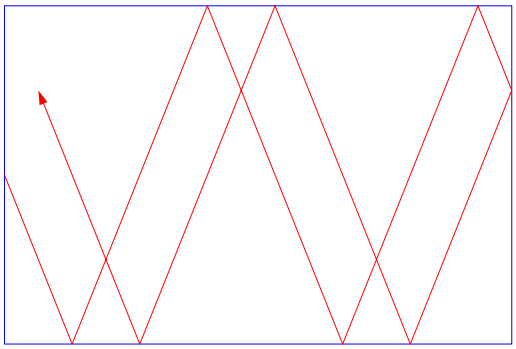

Figure 2: *The rectangle billiard*

The dynamical behavior of a billiard is determined by the properties of the boundary ∂Q, and it may vary greatly from completely regular or integrable to strongly chaotic. For example, the dynamics in simple containers (like circles or rectangles as shown in Figure 2) are integrable, the trajectories can be computed analytically and easily.

The first chaotic billiards were discovered by Sinai [20], who examined systems of dispersing type corresponding to the case when ∂Q is the union of a finite number of concave pieces (concave boundaries, by convention, refer to boundary curves with centers of curvature lying outside of Q). Two standard examples of billiards of this type are (as shown in Figure 3.a) on the 2D-torus with a finite number of scatterers made up of disjoint convex regions and (like in Figure 3.b) those on planar domains.

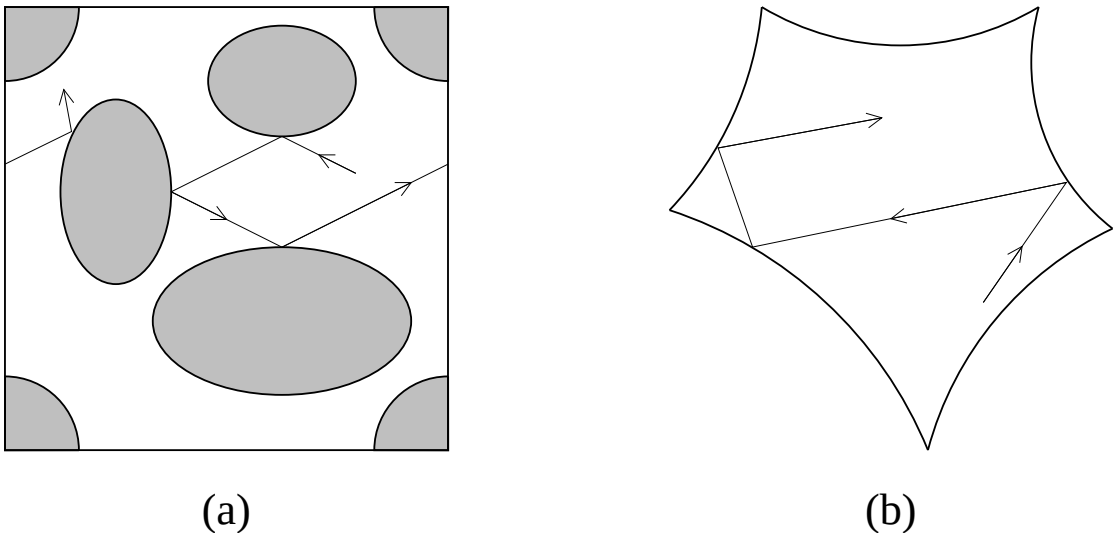

Figure 3: *Dispersing billiards*

Sinai proved that the dynamics are hyperbolic, ergodic and mixing in the mentioned billiards. Later on, such properties were proven in cases of other families of billiards: Bunimovich [3, 4] in the 1970s, Wojtkowski [22], Markarian [16], Donnay [13], and again Bunimovich [5] in the 1980s and early 1990s (and many others since) have greatly contributed to the subject.

As one can see, even the ergodic properties of billiards have kept mathematicians busy for over the past 35 years, though ergodicity is a very weak property. The correlation functions' rate of decay is much finer, has a lot higher physical meaning and importance (see Section 3.1.1), though it is more difficult to study.

The subject of this study is a special family of billiards that resemble the squash vegetable and a special case of it called the Bunimovich stadium. We will discuss their main properties, examine the decay of various correlation functions, and try to find suitable explanations for the observed phenomenon.

2 The "squash" billiard

The billiard to be studied in the latter is defined as follows: Consider a Q subset of $\mathbb{R}^2$, where ∂Q consists of two arcs of circles, one with the radius of r, the other with R, with centers placed at a distance d. The arcs are connected by their common outer tangent of length L (see Fig. 4). There is only one "ball" that reflects off the boundary elastically.

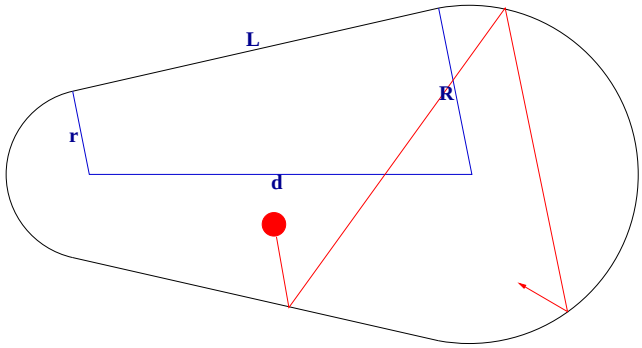

Figure 4: *The "squash" billiard*

The so called Bunimovich stadium is a special case of the squash billiard, where the radii of the arcs are equal (Figure 5). The mathematically rigorous investigation of the stadium started with [4] where Bunimovich showed (with respect to the natural invariant measure) that the Lyapunov exponents are almost everywhere non-zero, and that the system is ergodic. Non-dispersing billiards such as the squash only produce hyperbolicity when certain conditions are met: Even though nearly parallel rays first become convergent, they diverge after focusing, and expansion in phase space results if, before the next collision, they have diverged more than they have converged. See [22] for precise formulations.

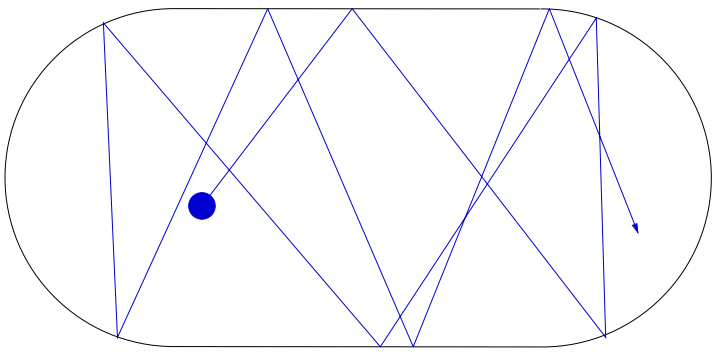

Figure 5: *The Bunimovich stadium*

By the state of the ball, we will mean its location on the plane ($\underline{x} \in Q$) and the unit vector that gives us the exact direction of its velocity ($\underline{u}$) (as it is shown on Figure 6).

We study the process in discrete time, where one step corresponds to one collision, so the state at the n-th step can be determined by the coordinates of the collision and the direction of the outgoing velocity.

The process can be described by the evolution of two coordinates (l, α) instead of the four (x_1, x_2, u_1, u_2), where l gives us the arc length parameter along the boundary and α is the angle of reflection (to the normal of ∂Q) (see Figure 7). The coordinate l will be 0 at the meeting point of the left arc and the lower line, and will grow counterclockwise. The angle α also grows counterclockwise, from $-\pi/2$ to $\pi/2$.

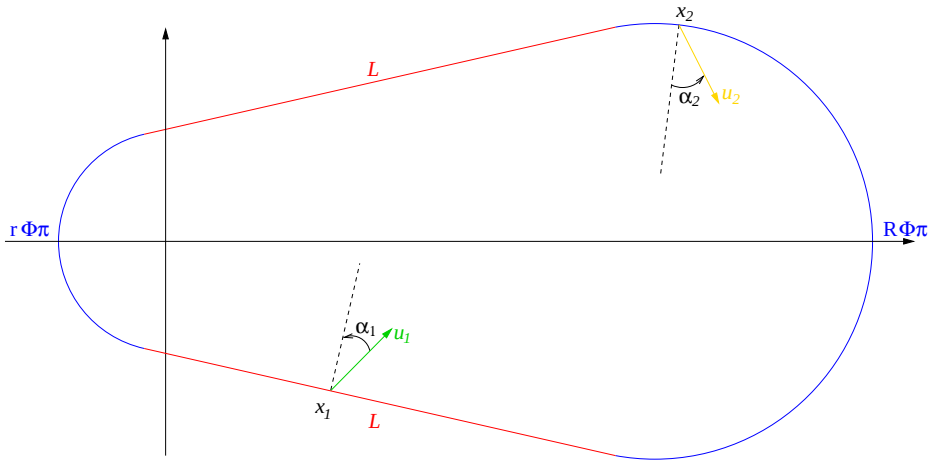

Figure 6: *The four dimensional model.*

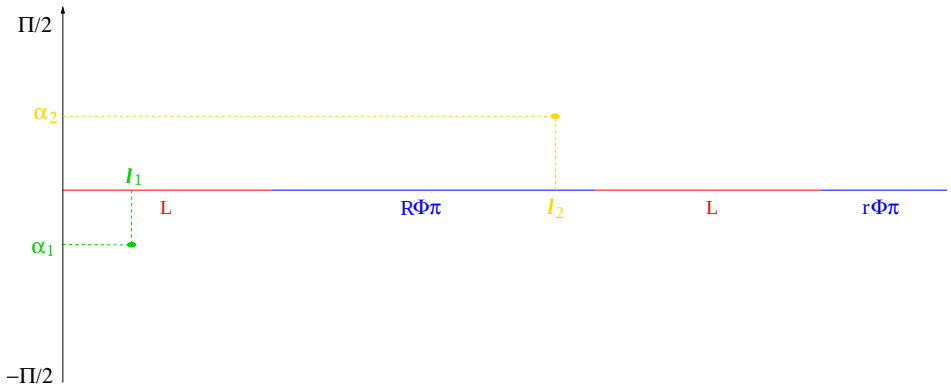

Figure 7: *The two dimensional phase space.*

Both of the above two notations are used throughout the thesis, as the (l, α) coordinates are more convenient for a theoretical approach, however it is more transparent to work directly with the locations and the velocities when programming simulations.

All of the functions and maps defined later (f, T, f_n, T^n) could be expressed both in terms of the two and of the four coordinates. We shall use the same notations for the resulting objects, this should cause no confusion.

2.1 The dynamics: definitions

I will only use the two dimensional convention here.

Let $M = \partial Q \times [-\frac{\pi}{2}, \frac{\pi}{2}]$ be the state space. Given $x = (l, \alpha) \in M$, consider the billiard trajectory starting out of x with the velocity given by α, and denote $Tx = (l', \alpha') \in M$, where l' is the location and α' is the outgoing velocity at the next moment of collision. Defined this way, we think of the map $T : M \to M$ and its higher iterates $T^n : M \to M$ as a discrete time dynamical system. As we shall see in Section 2.2, there is a convenient measure μ preserved by T. Let $f : M \to \mathbb{R}$ be a real-valued measurable function. The following functions can be thought of as random variables, and define a stationary stochastic process with $(M; \mu)$ as the underlying probability space (stationarity following from the invariance of the measure μ):

$$f_n = f \circ T^n, \qquad n \in \mathbb{Z}\,. \tag{2.1}$$

2.2 The invariant measure

The billiard dynamics preserves a natural measure on the phase space, that is absolutely continuous with respect to the Lebesgue measure.

Lemma 2.1 *The billiard map T preserves the smooth measure $\mathrm{d}\mu = \mathrm{d}l\mathrm{d}\alpha \cos\alpha$ on M.*

Proof Let us consider two consecutive moments of collision and introduce the following notations:

- Let (l, α) be the first state,
- (l', α') be the second state, and
- Φ be the angle of the two normal vectors of the boundary-segments where the collisions occur.

One can easily see that $\alpha' = \Phi - \alpha$, for the angles $\pi/2 - \alpha$, $\pi/2 - \alpha'$ and Φ add up to π because they form the angles of a triangle (see Figure 8).

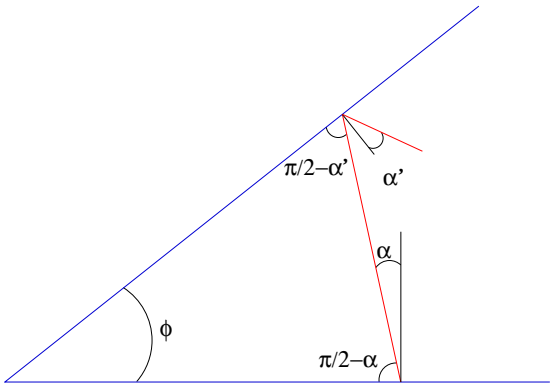

Figure 8: *The angles* $\pi/2-\alpha$, $\pi/2-\alpha'$ *and* Φ *total up to* π.

Neglecting the higher order terms, it can also be seen that (according to the sine theorem)

$$\frac{\partial l'}{\partial l} = \frac{\sin(\frac{\pi}{2}-\alpha)}{\sin(\frac{\pi}{2}+\alpha-\Phi)} = \frac{\cos(\alpha)}{\cos(\alpha-\Phi)} \,, \tag{2.2}$$

and

$$\partial\alpha' = (\Phi+\alpha+\partial\alpha)-(\Phi+\alpha) = \partial\alpha \,. \tag{2.3}$$

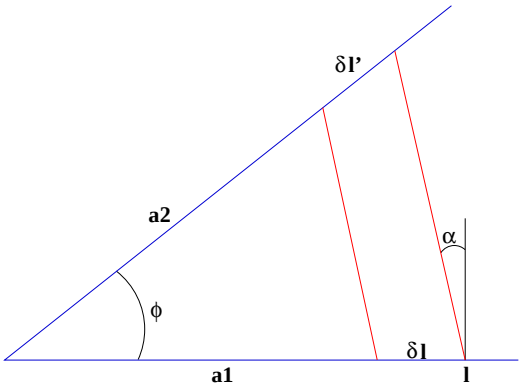

Figure 9: *The change of* ∂l

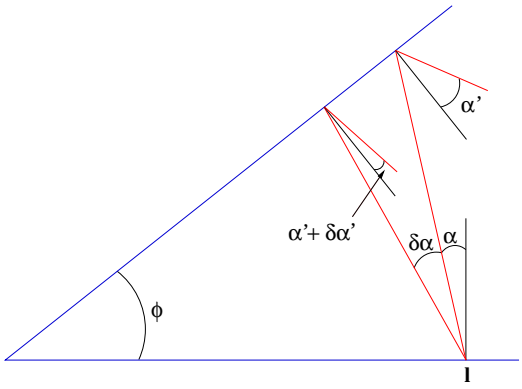

Figure 10: *The change of* $\partial\alpha$

Since $\partial\alpha'$ doesn't depend on ∂l up to first order, $\frac{\partial\alpha'}{\partial l} = 0$, which is enough information for us to derive the following Jacobian:

$$\begin{vmatrix} \frac{\partial l'}{\partial l} & \frac{\partial l'}{\partial\alpha} \\ \frac{\partial\alpha'}{\partial l} & \frac{\partial\alpha'}{\partial\alpha} \end{vmatrix} = \begin{vmatrix} \frac{\cos(\alpha)}{\cos(\alpha-\Phi)} & \frac{\partial l'}{\partial\alpha} \\ 0 & 1 \end{vmatrix} = \frac{\cos(\alpha)}{\cos(\alpha-\Phi)} = \frac{\cos(\alpha)}{\cos(\alpha')} \,, \tag{2.4}$$

which finally proves that

$$\partial l'\partial\alpha'\cos(\alpha') = \partial l\partial\alpha\cos(\alpha) \,. \tag{2.5}$$

3 Decay of correlations

3.1 The correlation functions

The everyday meaning of the correlation is how much two variables depend on each other. Given two $\mathbb{L}^2$ random variables X and Y, their correlation $Corr(X,Y)$ is defined as

$$Corr(X,Y) = \frac{\mathbb{E}(XY) - \mathbb{E}(X)\mathbb{E}(Y)}{\mathbb{D}(X)\mathbb{D}(Y)}\,, \tag{3.1}$$

where $\mathbb{E}$ stands for the expectation value and $\mathbb{D}$ is the deviation.

Let $f, g \in \mathbb{L}^2_\mu(M)$ be functions. The *time correlation function* [7] of f and g is defined in analogy with equation (3.1), as follows:

$$C_{f,g}(n) = \frac{\mathbb{E}(f \cdot (g \circ T^n)) - \mathbb{E}(f)\mathbb{E}(g)}{\mathbb{D}(f)\mathbb{D}(g)}\,, \tag{3.2}$$

where

$$\mathbb{E}(f) = \int_M f \mathrm{d}\mu, \qquad \text{and} \qquad \mathbb{D}(f) = \sqrt{\mathbb{E}(f^2) - \mathbb{E}(f)^2}\,. \tag{3.3}$$

This function measures the dependence between the values of f at time 0 and of g at time n.

It is also common to study the asymptotics of correlation functions more specific than (3.2), namely

$$C_f(n) = \frac{\mathbb{E}(f \cdot (f \circ T^n)) - \mathbb{E}^2(f))}{\mathbb{D}^2(f)}\,, \tag{3.4}$$

This function measures the dependence of two observations with a time gap n. The function $C_f(n)$ in (3.4) is called an *autocorrelation function.*

Let us now relate the expressions defined above to some of the standard notions in ergodic theory. Recall that a dynamical system (M, T^n, μ) is said to be *mixing* if for any two measurable sets $A, B \subset M$, we have $\mu(A \cap T^{-n}B) \to \mu(A)\mu(B)$ as $n \to \infty$. The following fact is standard in ergodic theory:

Lemma 3.1

$$C_{f,g}(n) \to 0 \text{ as } n \to \infty \text{ for all } f, g \in \mathbb{L}^2(M) \text{ if and only if } (M, T^n, \mu) \text{ is mixing.} \tag{3.5}$$

This means that the two quantities asymptotically become independent. In the case where $f = g$, the faster $C_f(n)$ tends to zero, the closer f_n and f are to an i.i.d setting.

The rate of the correlation decay (or the speed with which $C_f(n)$ tends to 0 as $n \to \infty$) is the property we will study for various f functions. Of course when examining the decay rate, dividing by the variance will have no effect on the order of magnitude of the outcome, since it is only a constant.

The order of the decay can of course differ when using different functions. For example when $f(x) \equiv c$ μ-almost surely, where c is an arbitrary constant, $C_f(n) \equiv 0$. Fast-decaying functions can always be found, so my aim will be to find an upper bound by using functions that are not exceptional at first sight.

According to [8], the functions for which the upper bound can be given relatively easily are the piecewise Hölder-continuous functions. In the case of typical piecewise Hölder-continuous functions, this bound turns out to be sharp, however there exists a degenerate family of functions that corresponds to the coincidence of certain averages, for which the decay rate is faster [2].

3.1.1 Why study correlation functions?

The rate of correlation decay for various functions can tell much about the dynamics of the system studied. Let me mention one particular example.

For $n \geq 0$, let $S_n : M \to \mathbb{R}$ be the ergodic sum of f_n [7]. That is,

$$S_n = \sum_{k=0}^{n-1} f \circ T^k \, . \tag{3.6}$$

The function S_n/n is the time average of the process f_n. The Birkhoff Ergodic Theorem asserts that if (M, T^n, μ) is ergodic and f is integrable, then S_n/n converges almost surely to $\mathbb{E}(f)$ as $n \to \infty$. (In probability theory, this is also called the strong law of large numbers.)

Next, we say that f_n satisfies the central limit theorem (CLT) if

$$\lim_{n\to\infty} \nu\left(\frac{S_n - n\mathbb{E}(f)}{\sqrt{n}} < z\right) = \frac{1}{\sqrt{2\pi}\sigma} \int_{-\infty}^{z} e^{-\frac{s^2}{2\sigma^2}} \mathrm{d}s \tag{3.7}$$

for all $-\infty < z < \infty$, where ν is the invariant probability measure of the system. Here $\sigma = \sigma_f \geq 0$ is a constant. (In the case $\sigma_f = 0$, the right side of the equation is to be read as 0 for $z < 0$ and 1 for $z > 0$.) Equation (3.7) is equivalent to the convergence of $(S_n - n\mathbb{E}(f))/\sqrt{n}$ in distribution to the normal random variable $N(0, \sigma_f^2)$. I remark that the central limit theorem is considerably much finer statement than the Birkhoff Ergodic Theorem; it tells us that the distribution of the fluctuations of the time average S_n around its mean value $n\mathbb{E}(f)$, when divided by $\sqrt{n}$, is asymptotically Gaussian (even when S_n is not a sum of i.i.d. variables).

Lemma 3.2 *The variance σ_f^2 in the CLT is related to the correlation function (3.4) by*

$$\sigma_f^2 = C_f(0) + 2\sum_{n=1}^{\infty} C_f(n) \ . \tag{3.8}$$

Proof For simplicity, let $\mathbb{E}(f) = 0$ and $\mathbb{D}(f) = 1$. This way, the variance of $\frac{S_n - n\mathbb{E}(f)}{\sqrt{n}}$ can be calculated in the following way:

$$\mathbb{E}\left(\frac{S_n^2}{\sqrt{n}^2}\right) = \mathbb{E}\left(\frac{(f + f\circ T + \ldots f\circ T^{n-1})^2}{n}\right) =$$

$$\frac{1}{n}\mathbb{E}\left(\sum_{i=0}^{n-1}(f\circ T^i)^2 + \sum_{i\neq j}(f\circ T^i)(f\circ T^j)\right) =$$

$$= \frac{1}{n}\left(\sum_{i=0}^{n-1}\mathbb{E}((f\circ T^i)^2) + 2\sum_{i<j}\mathbb{E}((f\circ T^i)(f\circ T^j))\right) \ .$$

Because of the invariance of the measure, this is equal to

$$= \frac{1}{n}n\mathbb{E}(f^2) + \frac{2}{n}\sum_{l=1}^{n-1}\mathbb{E}(f(f\circ T^l))(n-l)$$

$$= \frac{1}{n}n\mathbb{E}(f^2) + \frac{2}{n}\sum_{l=1}^{n-1}\mathbb{E}(f(f\circ T^l))n - \frac{2}{n}\sum_{l=1}^{n-1}\mathbb{E}(f(f\circ T^l))l \ .$$

If $\sum_{l=1}^{\infty} C_f(l) < \infty$, then $\sum_{l=1}^{n-1} C_f(l)l = o(n)$, so $\frac{2}{n}\sum_{l=1}^{n-1}\mathbb{E}(f(f\circ T^l))l \to 0$, from which we can finally obtain that as $n \to \infty$, the amount above tends to

$$C_f(0)^2 + 2\sum_{l=1}^{\infty} C_f(l) \ .$$

It follows that a prerequisite for the central limit theorem is the summability of the correlation function $C_f(n)$. Most existing proofs of the CLT for dynamical systems follow essentially (though not immediately) from slightly stronger estimates on the speed of correlation decay.

Further information on issues related to the central limit theorem or other limit theorems for dynamical systems can be found in [12] and in [2].

3.2 The rate of the decay

Today there are many rigorous results available in the subject of correlation decay in billiards. Among the first, I can specifically mention the work of Bunimovich and

Sinai, who proved that the velocity autocorrelation function $C_v(n)$ of a particle in a dispersing billiard with periodic configuration of scatterers and uniformly bounded free path exhibits a stretched exponential decay rate [6]:

$$C_v(n) \leq e^{-\alpha n^\beta} \ , \tag{3.9}$$

where $\alpha > 0$ and $0 < \beta \leq 1$. This was corrected by Young, who proved that β was indeed 1, so the rate was exponential [23].

All hyperbolic systems are characterized by exponential instability of motion (due to the non-zero Lyapunov exponents, see Section 4.3), which in turn implies that the memory of the initial state is lost exponentially fast. For this reason, it has been conjectured that the correlation should also always decay in an exponential fashion in all of these systems.

This widespread belief was shaken by the work of Alder and Wainwright in 1970 [1], who numerically detected the existence of decays with tails heavier than exponential in the hard-sphere gas. The difference between dispersing billiards with uniformly bounded free paths and the hard-sphere gas is that the first one is uniformly hyperbolic, while the second one is not. This is because the latter may contain certain trajectories that do not collide with dispersing surfaces (that is, a particle avoids the others) and which can be of any length, causing segments of (in a sense) simple motion in the trajectories.

Later on, Vivaldi, Casati and Guarneri have presented a heuristical explanation for such a phenomenon in the stadium, in 1983 [21]. (The stadium is similar to the hard-sphere gas, for it also contains regular segments of trajectories, see Section 3.3.) They were the first to state that the source of long-time tails is to be sought in the presence of the arbitrarily long segments of regular motion in the time evolution of a stochastic orbit. These motions are locally integrable (for the particular case of the $2D$ billiards studied here, the angle of reflection remains unchanged), and will be referred to as *integrable segments* of trajectories.

The case of the squash billiard (in this point of view) is qualitatively different from that of the stadium, for the geometric properties that cause the appearance of integrable segments are not the same (see Figures 11 and 12).

Here I will present a different heuristical approach which I will use to determine the speed of the decay for the indicator function of the straight lines in the stadium, and of a subset of the large arc in the squash.

3.3 Measure of the capture regions

In the stadium's case, the regular segments of trajectories can be seen in figure 11 [21]. I shall refer to the alternate collisions between the two opposite line segments as case 1, and to the consecutive collisions within the same arc as case 2.

Let us define $M_i^n \subset M$ for $i = 1, 2$ corresponding to these two cases as the sets of initial conditions starting out of which the trajectories follow these integrable patterns exactly up to the first n iterations. The sets M_i^n will be referred to as *capture regions* of order n.

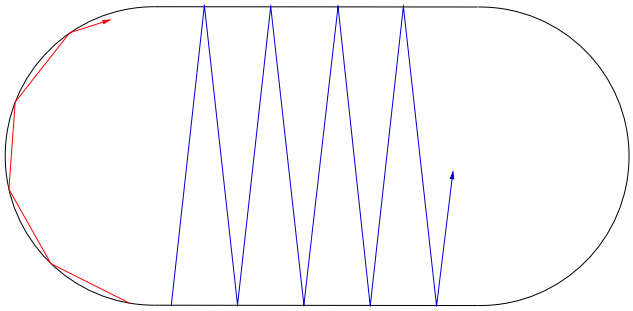

Figure 11: *Long regular motion in the stadium billiard*

In the case of the squash, as one of the two circular arcs is larger than a semi-circle, a new type of capture region can be identified: it corresponds to motion close to the diameter of this arc, which will be referred to as case 3. The capture that corresponds to the alternating bounces between the two line segments disappears as they are no longer parallel, however the effect that is responsible for M_2^n in the stadium is present here also: case 4 will mean rolling along the arcs.

Analogously, the long regular trajectories that define the capture regions in the squash can be found along the arcs (M_4^n) and across the larger arc (M_3^n) as shown in Figure 12.

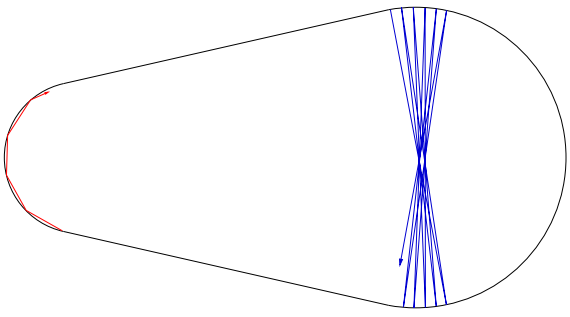

Figure 12: *Types of long regular motion in the squash billiard*

3.3.1 The stadium: bouncing between the line segments

This case is more important, for as we will see, the measure of the region M_1^n is of higher order in n. It is enough to consider the points of the lower line only, as this set appears symmetrically on the two parallel lines. We will simply need to multiply the resulting measures by the number of occurences in the phase space.

First of all, to belong to M_1^n, i.e. to be the starting point of an integrable segment of length n, we should ensure that the preimage of the point is on one of the semicircles, otherwise it would only be an intermediate point of a longer segment.

If a ball has just arrived to the lower line, its angle of incidence has to be in the range shown on Figure 13. Note that the velocity coordinate is the angle of reflection, so the points that represent these trajectories are positioned in the phase space of the stadium as seen on Figure 14. I shall refer to this area as the first arrival subset.

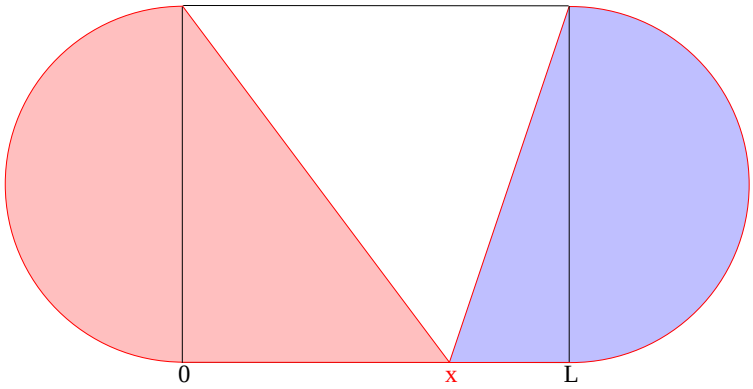

Figure 13: *The range of directions from which the particle can arrive from.*

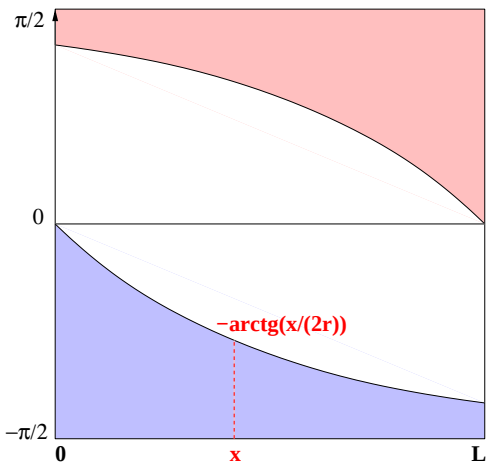

Figure 14: *The first arrival subset of the straight lines on the phase space.*

This means that α has to satisfy one of the following inequalities:

$$\begin{aligned} \alpha &\leq -\operatorname{arctg} \tfrac{x}{2r} \\ \alpha &\geq \operatorname{arctg} \tfrac{L-x}{2r} \ . \end{aligned} \tag{3.10}$$

Now we may proceed and determine the subset containing the points that are on the lower line now and will be bouncing between the two lines for exactly the next n steps:

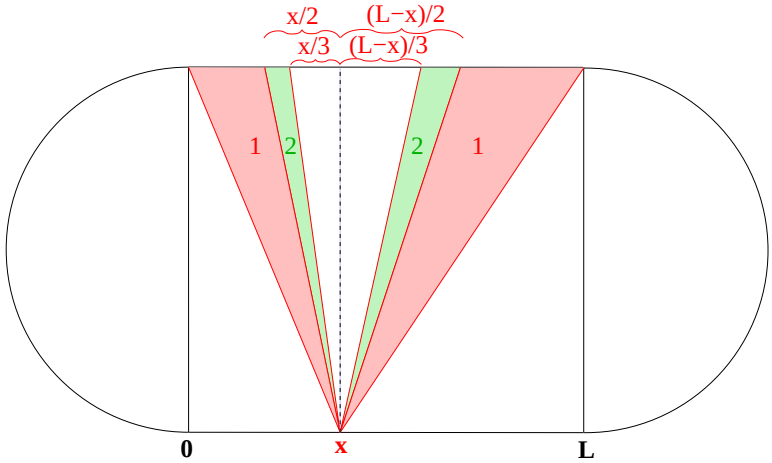

Figure 15: *The directions in which the particle will collide once or twice.*

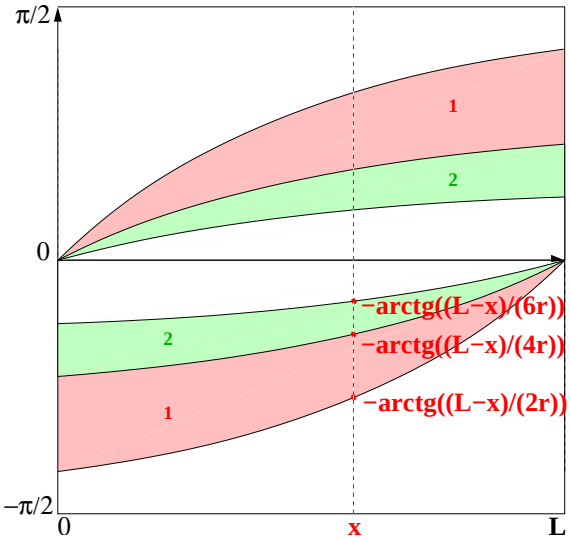

Figure 16: *The same directions given on the phase space.*

The points that will only collide once with the lines and then leave them should have an outgoing velocity within the red region shown on Figure 15. Similarly one can determine the places starting out of which the ball will bounce $2, 3, 4$, etc... times, which leads us to the inequalities (3.11) and to the regions in the phase space as on Figure 16:

$$\begin{cases} \alpha_n \leq \operatorname{arctg} \frac{x}{2rn} \\ \alpha_n \geq \operatorname{arctg} \frac{x}{2r(n+1)} \end{cases} \text{, or } \begin{cases} \alpha_n \leq -\operatorname{arctg} \frac{L-x}{2r(n+1)} \\ \alpha_n \geq -\operatorname{arctg} \frac{L-x}{2rn} \end{cases} . \tag{3.11}$$

where x is the arc length distance of our point from the intersection point of the lower line and the left arc, and α_n is a possible angle of reflection that results in n collisions *exactly* (not counting the starting point).

The line separating the regions that correspond to (neglecting the first collision) $n-1$ and n times bouncing trajectories shall be called *singularity line* of order n.

The points in the phase space that represent the beginning of trajectories that bounce *at least* $n+1$ times (with the first collision counted) are contained in the intersections of the areas described in Figures 14 and 16 (see Figure 17).

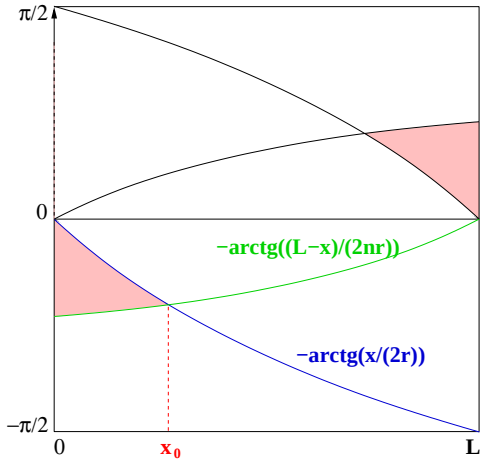

Figure 17: *The intersection of the* arctg *curves.*

The measure of the capture regions can be calculated as

$$\mu(M_1^n) = \int_{M_1^n} \mathrm{d}\mu = \int_{M_1^n} cos\alpha \mathrm{d}\alpha \mathrm{d}x \, . \tag{3.12}$$

As n is large, α is close to 0, so the function $\cos\alpha$ is approximately 1. Because of this, one can estimate the measure of the capture region M_1^n by calculating the Lebesgue measure. The $\operatorname{arctg} y$ functions can also be replaced by y when y is small, so the area that is bounded by the arctg curves (Figure 17) containing the starting point of trajectories that bounce at least $n+1$ times all together is close to a triangle.

The location of the intersection point x_0 can be estimated by solving the equation $\frac{x_0-L}{2nr} = -\frac{x_0}{2r}$. From this, we get $x_0 = \frac{L}{n+1}$.

This way we can calculate the measure of the capture regions up to first order (the factor 4 is needed as the same picture appears four times in the phase space, twice on both of the two lines).

$$\frac{1}{4}\mu\left(\bigcup_{k\geq n+1} M_1^k\right) \approx \frac{1}{2}\left(\frac{L}{2nr}\right) x_0 = \frac{1}{2}\left(\frac{L}{2nr}\right)\frac{L}{n+1} = \frac{L^2}{4rn(n+1)} \tag{3.13}$$

The asymptotic measure of M_1^n is readily obtained from 3.13 as

$$\mu(M_1^n) \approx \mu\left(\bigcup_{k\geq n} M_1^k\right) - \mu\left(\bigcup_{k\geq n+1} M_1^k\right) = 4\left(\frac{L^2}{4rn(n-1)} - \frac{L^2}{4rn(n+1)}\right) =$$

$$= \frac{2L^2}{r(n-1)n(n+1)} \approx \frac{2L^2}{rn^3}\ . \tag{3.14}$$

3.3.2 The stadium: rolling along one of the arcs

Let us now show that the measure of the subset that is responsible for the effect of rolling along an arc for over n steps is of lower order than the previously discussed one.

If the particle is hitting the arc for the first time, its angle of reflection has to be inside the illustrated range of width $\pi/2$ (Figure 18).

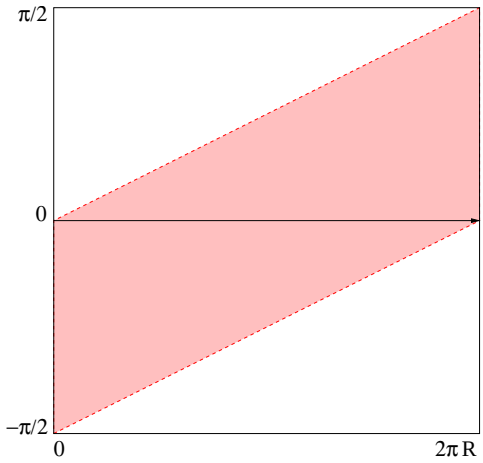

Figure 18: *The first arrival subset of the case 2 trap.*

The points on the phase space that are on one of the arcs and will collide with the same arc for *exactly* n more times belong to the triangle-shaped areas shown on Figure 19. Note that the subsets where the particles will roll for *at least* n steps are right angle triangles with the singularity line of order n as the hypotenuse.

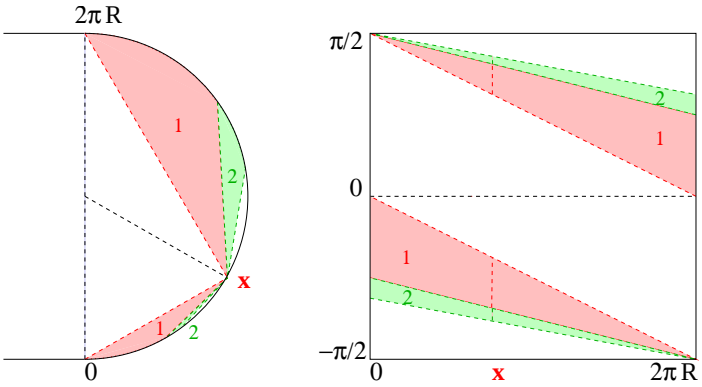

Figure 19: *The range of the angles which will result in exactly* 1 *or* 2 *collisions along the arc (not counting the arriving point).*

Similarly to the case of Section 3.3.1, we will calculate the measure of these triangles intersected with the first arrival subset (Figure 20). It is adequate to regard one (the lower left) triangle only, since the system has its symmetries.

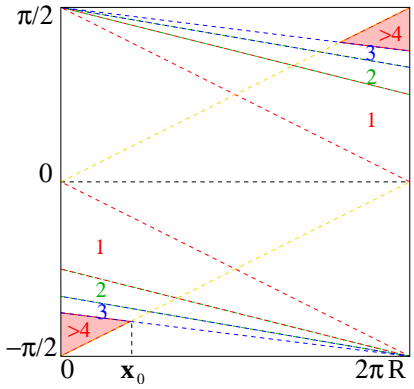

Figure 20: *The intersection of the subsets described in Figures 18 and 19.*

The equation of the line forming the upper right sides of the triangle is $\alpha = -\frac{\pi}{2} + \frac{\pi}{2n} - \frac{x}{2nr}$, while the lower right edge's is $\alpha = -\frac{\pi}{2} + \frac{x}{2r}$. The intersection point x_0 can be determined easily:

$$\begin{aligned} -\tfrac{\pi}{2} + \tfrac{\pi}{2n} - \tfrac{x_0}{2nr} &= -\tfrac{\pi}{2} + \tfrac{x_0}{2r} \\ x_0 &= \tfrac{r\pi}{n+1} \end{aligned} \quad . \tag{3.15}$$

Thus, the exact measure of one of the four triangles will be as follows:

$$\frac{1}{4}\mu\left(\bigcup_{k\geq n+1} M_2^k\right) = \int_0^{\frac{r\pi}{n+1}} \int_{-\frac{\pi}{2}+\frac{x}{2r}}^{-\frac{\pi}{2}+\frac{\pi}{2n}-\frac{x}{2nr}} \cos\alpha \mathrm{d}\alpha \mathrm{d}x = \int_0^{\frac{r\pi}{n+1}} \cos\frac{x}{2r} - \cos\left(\frac{\pi}{2n} - \frac{x}{2nr}\right) \mathrm{d}x =$$

$$= 2r\sin\frac{\pi}{2(n+1)} + 2nr\sin\left(\frac{\pi}{2n} - \frac{\pi}{2n(n+1)}\right) - 2nr\sin\frac{\pi}{2n} \; . \tag{3.16}$$

When n is large, $\sin\frac{const}{n}$ can be approximated to the third order using its Taylor polynomial in $\frac{1}{n}$:

$$\approx 2r\left(\frac{\pi}{2(n+1)}-\frac{1}{3!}\left(\frac{\pi}{2(n+1)}\right)^3\right)+$$

$$2nr\left(\frac{\pi}{2n}-\frac{\pi}{2n(n+1)}-\frac{1}{3!}\left(\frac{\pi}{2n}-\frac{\pi}{2n(n+1)}\right)^3\right)-2nr\left(\frac{\pi}{2n}-\frac{1}{3!}\left(\frac{\pi}{2n}\right)^3\right)=$$

$$\frac{r\pi^3}{24}\left(\frac{2n+1}{n^2(n+1)^2}\right)\approx\frac{r\pi^3}{12}\left(\frac{1}{n(n+1)^2}\right)\ , \tag{3.17}$$

from which we obtain

$$\mu(M_2^n)=\mu\left(\bigcup_{k\geq n}M_2^k\right)-\mu\left(\bigcup_{k\geq n+1}M_2^k\right)\approx\frac{r\pi^3}{3}\left(\frac{1}{(n-1)n^2}\right)-\frac{r\pi^3}{3}\left(\frac{1}{n(n+1)^2}\right)=$$

$$=\frac{r\pi^3}{3}\left(\frac{3n+1}{(n-1)n^2(n+1)^2}\right)\approx\left(\frac{r\pi^3}{n^4}\right)\ . \tag{3.18}$$

3.3.3 The squash: across the larger arc

I will use the convention that regards only the indicated parts of the larger arc as the trap (see Figure 21).

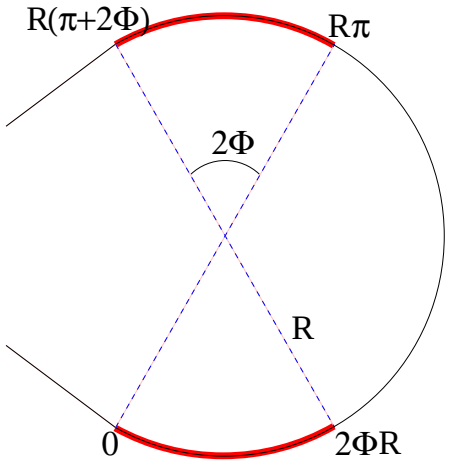

Figure 21: *The case 3 trap.*

The following figure shows the first arrival subsets: The red domain contains the arriving points to the whole large arc, while the blue regions represent the points coming from the inner part of the arc into the trap.

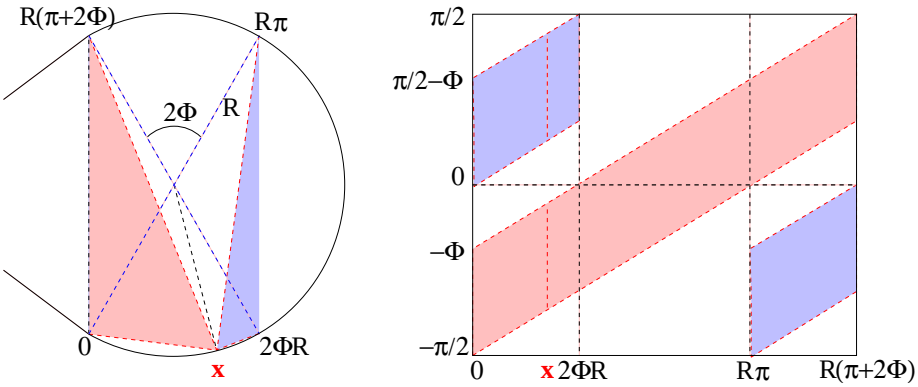

Figure 22: *The incoming directions of the first arriving trajectories and their hitting points in the phase space.*

Again, we need to approximate the order of the measure of points beginning from which the trajectories complete series of bounces between the two opposite sides of the larger arc of length n exactly.

In order to do this, we need to estimate the measure of the triangles which can be obtained by intersecting the first arrival subset with the triangles that include the starting point of trajectories that will bounce n times.

The blue triangles in Figure 23, for example, include the points corresponding to trajectories that perform at least 3 consecutive bounces in the trap.

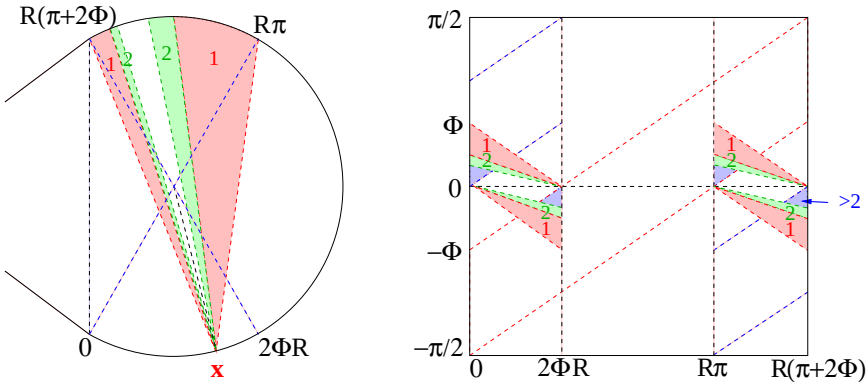

Figure 23: *The directions in which a trajectory starting from x will collide once or twice, and the regions that contain these points on the phase space. The intersections with the first arrival set are indicated as well.*

I will only consider the lower left triangle (so we will get $\frac{1}{4}\mu\left(\bigcup_{k\geq n+1} M_3^k\right)$), where the upper left edge's equation is $\alpha = -\Phi + \frac{x}{2R}$, and the lower left one is $\alpha = -\frac{x}{2nR}$. Their intersection point x_0 is obtained from $-\Phi + \frac{x}{2R} = -\frac{x}{2nR}$, so

$$x_0 = \frac{2Rn\Phi}{n+1}\,. \tag{3.19}$$

$$\frac{1}{4}\mu\left(\bigcup_{k\geq n+1} M_3^k\right) = \int_{\frac{2Rn\Phi}{n+1}}^{2\Phi R}\int_{-\frac{x}{2nR}}^{-\Phi+\frac{x}{2R}} \cos\alpha \mathrm{d}\alpha \mathrm{d}x =$$

$$= 2R\left(-1 - n\cos\left(\frac{\Phi}{n}\right) + \cos\left(\frac{-\Phi}{n+1}\right) + n\cos\left(\frac{\Phi}{n+1}\right)\right) . \tag{3.20}$$

When n is large, we can continue by approximation:

$$\approx 2R\left(-1 - n\left(1 - \frac{1}{2}\left(\frac{\Phi}{n}\right)^2\right) + \left(1 - \frac{1}{2}\left(\frac{\Phi}{n+1}\right)^2\right)\right) + n\left(1 - \frac{1}{2}\left(\frac{\Phi}{n+1}\right)^2\right) =$$

$$= \frac{R\Phi^2}{n(n+1)} . \tag{3.21}$$

This gives us the measure of M_3^n:

$$\mu(M_3^n) = \mu\left(\bigcup_{k\geq n} M_3^k\right) - \mu\left(\bigcup_{k\geq n+1} M_2^k\right) \approx \frac{4R\Phi^2}{(n-1)n} - \frac{4R\Phi^2}{n(n+1)} =$$

$$= \frac{8R\Phi^2}{(n-1)n(n+1)} \approx \frac{8R\Phi^2}{n^3} . \tag{3.22}$$

3.3.4 The squash: rolling along the arcs

The measure of the subset M_4^n can be obtained in a way very similar to the procedure I have used in the second case (see Secion 3.3.2). Again, the outcome has the same order of

$$O\left(\frac{1}{n^4}\right) \tag{3.23}$$

thus the corresponding effects can be neglected compared to M_3^n, when n is large.

3.4 Estimating the correlation decay

3.4.1 The stadium and the indicator function of the trap

As I have already mentioned, the main contribution to the slowly decaying correlation is due to the effect corresponding to case 1, since M_1^n has a measure of higher order than the capture region M_2^n of case 2.

The argument below will rely on the following observation: Consider a trajectory that has just completed a series of n consecutive collisions with the parallel lines (where n is large). After experiencing one or two bounces on one of the circular arcs, another long series of bouncing will start. In other words, the particle will reenter the case 1 trap again.

More precisely, if we have a series of length n, that means that the tangent of the angle of reflection on the lines has to be about $\frac{L}{2nr}$. When y is small, the function $\tan(y) \approx y$, so we have

$$\alpha \approx \frac{L}{2nr} \ . \tag{3.24}$$

Since α can at most grow up to 3α, but will be at least $\frac{\alpha}{3}$, the length of this next series will be between $\frac{n}{3} + \mathcal{O}(1)$ and $3n + \mathcal{O}(1)$ (see Figure 24).

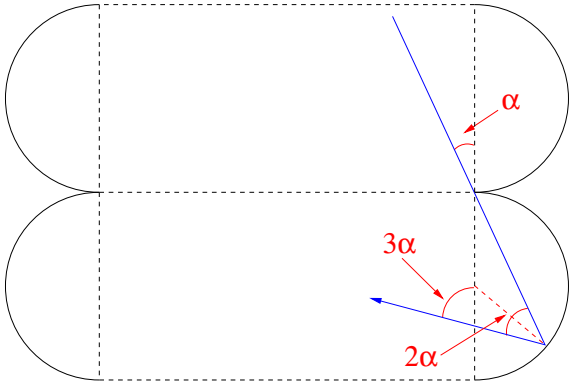

Figure 24: *The largest possible change of* α.

Let $R(n)$ be the random variable that tells the length of the next series, given the condition that the present bouncing segment is of length n with distribution determined by the measure μ', where μ' is the probability measure that can be obtained by normalizing μ:

$$\mu'(A) = \frac{\mu(A)}{2(2r\pi + 2L)} \ . \tag{3.25}$$

If $\frac{n}{3} < i < 3n$, then the probability of the event $R(n) = i$ is approximately $\frac{3n}{8i^2} + o(\frac{1}{i^3})$ [2].

The expected value can be obtained as follows:

$$\mathbb{E}(R(n)) \approx \sum_{i=n/3}^{3n} i\frac{3n}{8i^2} \approx n\frac{3}{4}\ln 3 \approx 0.824\ n \ , \tag{3.26}$$

which means that if a point has exited the trap after n steps, it will return for about $q_0 n$ bounces where $q_0 = \frac{3}{4}\ln 3$.

If a particle is in trap 1 for n steps (with n large) and reenters it after one or two bounces outside and keeps on doing this over and over, we shall say that the particle is in a *corridor*. The particle exits the corridor, once the number of consecutive collisions it makes inside the trap falls under some integer n_c.

Let X_0 be the part of the phase space that contains all points on the straight lines.

Let Y_n be the subset of the phase space that contains points which are now in X_0 and in a corridor, and which after n steps will still be inside the same corridor.

How can one measure something that is so vaguely defined? To approximate this latter quantity: If a point is inside Y_n, that means that n has to be less than the number of bounces it will make in the corridor all together. Note that not only the points of the first arrival subset are to be considered. For example if a point belongs to $T^{k-m}M_1^k$ with $m < k$, then it has m steps left of the k bounces in the trap. It is then likely to return to the trap and start a series of $q_0 k$ bounces. Thus n has to satisfy

$$n < m + \sum_{i=1}^{\infty} q_0^i k = m + \frac{q_0}{1-q_0} k \ , \tag{3.27}$$

where we have not counted the time spent outside of the trap, for that is an effect of lower order.

Knowing this, let us now estimate the measure of Y_n. According to equation (3.27), we add $\mu(M_1^k)$ as many times as the number of different values of m for a fixed k are allowed (See also Figure 25). We add the same amount for those parts of the phase space that correspond to phases somewhere in the middle of a bouncing sequence of length k, no matter how many collisions are still left ahead (the measure does not depend on m), because the mapping keeps the measure μ invariant.

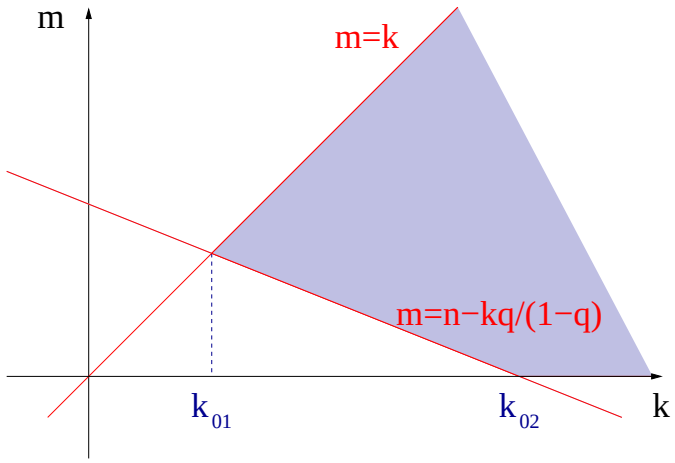

Figure 25: *The domain of the sum.*

$$\mu(Y_n) = \sum_{k=k_{01}}^{\infty} \sum_{m=max[0,\lceil n - \frac{q_0}{1-q_0} k \rceil]}^{k} \mu(M_1^k) = \sum_{k=k_{01}}^{k_{02}} \sum_{m=\lceil n - \frac{q_0}{1-q_0} k \rceil}^{k} \mu(M_1^k) + \sum_{k=k_{02}}^{\infty} \sum_{m=0}^{k} \mu(M_1^k) \ , \tag{3.28}$$

where $k_{01} = n(1-q_0)$ and $k_{02} = \frac{1-q_0}{q_0} n$ are the intersection points of the appropriate bounding lines. This yields

$$\mu(Y_n) \approx \sum_{k=(1-q_0)n}^{\frac{1-q_0}{q_0}n} \left(\frac{k}{1-q_0} - n\right) \mu(M_1^k) + \sum_{k=\frac{1-q_0}{q_0}n}^{\infty} k\mu(M_1^k) \approx$$

$$\sum_{k=(1-q_0)n}^{\frac{1-q_0}{q_0}n} \left(\frac{k}{1-q_0} - n\right) \frac{2L^2}{rk^3} + \sum_{k=\frac{1-q_0}{q_0}n}^{\infty} \frac{2L^2}{rk^2} \approx \frac{L^2(1+q_0)}{r(1-q_0)} \frac{1}{n} \,. \tag{3.29}$$

The first observable for which the correlation function was considered is the indicator function of the straight lines, that is

$$f_0(x) = \begin{cases} 1 & \text{if } x \in X_0; \\ 0 & \text{if not.} \end{cases} \tag{3.30}$$

By the definitions in (3.4), (3.25) and (3.30), the correlation function of $f(x)$ can be expressed as

$$C_{f_0}(n) = \frac{\mu'(X_0 \cap T^{-n}X_0) - \mu'(X_0)^2}{\mu'(X_0)(1-\mu'(X_0))} \,. \tag{3.31}$$

When intersecting $X_0 \cap T^{-n}X_0$ with Y_n, we get

$$C_{f_0}(n) = \frac{\mu'(Y_n \cap T^{-n}X_0) + \mu'((X_0/Y_n) \cap T^{-n}X_0) - \mu'(X_0)^2}{\mu'(X_0)(1-\mu'(X_0))} \,, \tag{3.32}$$

since $Y_n \subset X_0$.

By definition, the points in Y_n have to be in the corridor after n steps, which means that with a big probability (if n_c is large enough) they will also be on X_0, which allows us to write $\mu'(Y_n)$ instead of $\mu'(Y_n \cap T^{-n}X_0)$.

Another observation can be made: if n is appropriately big, then $\mu'((X_0/Y_n) \cap T^{-n}X_0)$ is about $\mu'(X_0/Y_n)\mu'(T^{-n}X_0)$. To see this, note that the points in X_0 that will exit the corridor in a time shorter than n will begin to lose their memory of the past exponentially fast (for the correlation in other parts of the phase space diminishes exponentially fast), thus being on X_0 after n collisions can be assured to be nearly independent of the location of the starting point.

Using these estimates, we have

$$C_{f_0}(n) \approx \frac{\mu'(Y_n) + \mu'((X_0/Y_n)\mu'(T^{-n}X_0) - \mu'(X_0)^2}{\mu'(X_0)(1-\mu'(X_0))} =$$

$$\frac{\mu'(Y_n) + \mu'((X_0/Y_n)\mu'(X_0) - \mu'(X_0)^2}{\mu'(X_0)(1-\mu'(X_0))} = \frac{\mu'(Y_n) - \mu'(Y_n)\mu'(X_0)}{\mu'(X_0)(1-\mu'(X_0))} =$$

$$= \frac{\mu'(Y_n)}{\mu'(X_0)} = \frac{\mu(Y_n)}{\mu(X_0)} \,. \tag{3.33}$$

Since $\mu(X_0) = 4L$, the result will be

$$\approx \frac{L(1+q_0)}{4(1-q_0)r}\frac{1}{n} \approx 2,59\frac{L}{rn} \ . \tag{3.34}$$

3.4.2 The squash and the indicator function of the trap

I will only consider the regular motion across the larger arc, for that defines the larger measure subset of the phase space.

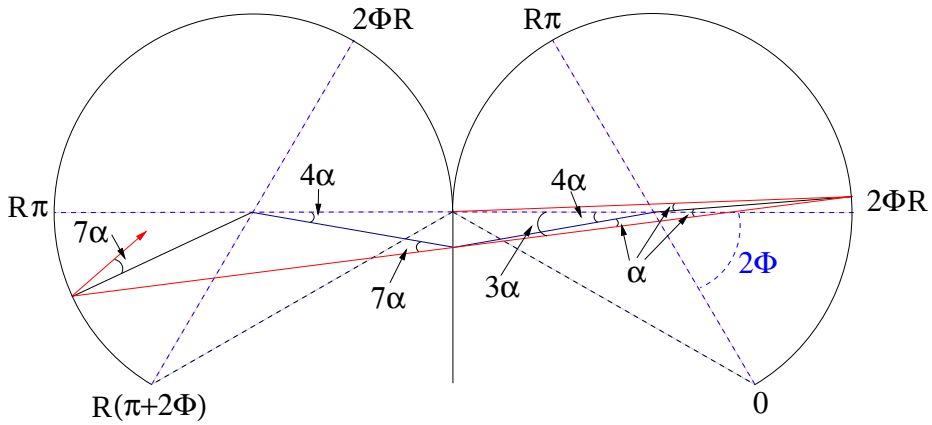

Figure 26: *The largest possible change of α when returning to the trap.*

Figure 26 shows the dynamics of a point starting from an extremal position: it is from here, that the point can land on the adjacent copy of the large arc with the greatest possible angle of incidence, given α. As one can see, the maximum of this angle is 7 times the original one (neglecting the effects of lower order). Because any trajectory can be realized in both the forward and the backward directions, this also leads to the fact that the minimum of the angle at the return will be $\alpha/7+\mathcal{O}(1)$. Since the absolute value of α is about $\frac{\Phi}{n} + \mathcal{O}(\frac{1}{n^2})$, it is only possible to return for a series of minimum $n/7 + \mathcal{O}(1)$ and maximum $7n + \mathcal{O}(1)$ bounces.

Let us now define the first return map τ of the map T: if a point x is anywhere in the phase space now, and the first time that it will hit the large arc right after colliding with some other parts of the boundary will be n collisions later, then $\tau(x) = T^n(x)$. We know, that the return dynamics are uniformly hyperbolic [8].

I will now examine the τ-images of the singularity lines and the domains bounded by them.

Let us redefine the singularity lines seen in Figure 23 in the following way:
The region of the phase space that will leave the large arc in the next moment of collision can be obtained by reflecting the first arrival subset to the line $\alpha = 0$ (the area bounded by the green dashed lines in Figure 27) and shall be referred to as the

exit domain. If I continue the singularity lines to their intersection with the boundary of this exit domain but only within the first arrival subset, I get regions containing all points that will be inside the trap for the *next* n steps and have just arrived to the large arc.

This way we cover the same measured regions as M_3^n, for the parts of the strips extending beyond the first arrival set correspond to T-preimages of pieces in M_3^n that were originally located on the upper left and on the lower right side of the phase space.

I will consider the bottom part of the trap only, for this trap is also symmetrical.

The τ-image of the domain introduced above consists of two parts. the lower side of the domain near the singularity line of order n will return after only one bounce on one of the straight lines, which means that if x is within this subset, $\tau(x)$ will again be inside a series. However if x is in the upper side, it will need an extra collision with the straight lines, that means that it is the second iterate, $\tau^2(x)$, that will begin the new series in the trap. According to [8], these images of the domain will be located in the phase space as in Figure 27. Thus we can see that the bounding lines of the images intersect the located singularity lines transversally.

The number of collisions a particle will experience when it is returning after completing a series of length n will depend on the τ-image of the point, that is, which domain among the M_3^i will it fall into.

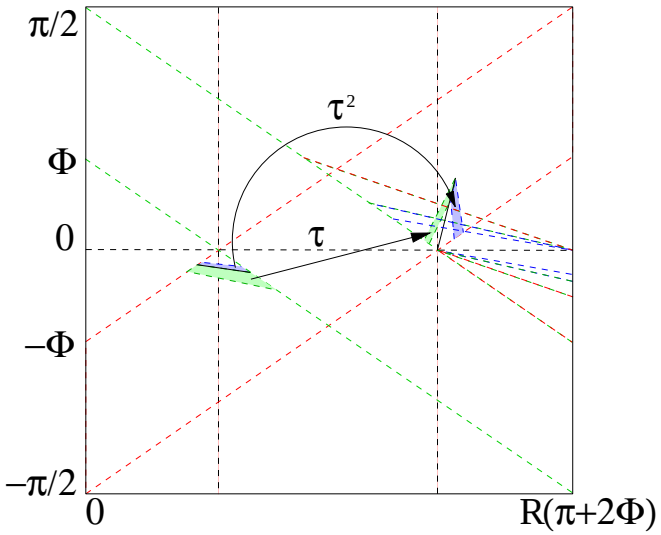

Figure 27: *The image of the domain containing the points of the arc that will complete a series of length n.*

Fix n large, and consider the image of a domain as in Figure 27. The singularity lines crossing such an image can be considered to be parallel. This allows us to determine the distribution of the length of the next series as follows: The probabilities $\mathbb{P}(n \to i)$

are proportional only to the height of the cell crossed by the image of the domain. Since $\mu(M_3^i) = \mathcal{O}(\frac{1}{i^3})$ and their width is $\mathcal{O}(\frac{1}{i})$, we know that

$$\mathbb{P}(n \to i) = \frac{c}{i^2} \, . \tag{3.35}$$

Now we may determine the number c:

$$\sum_{i=n/7}^{7n} \frac{c}{i^2} = 1 \tag{3.36}$$

thus we have

$$c = \frac{7n}{48} \, . \tag{3.37}$$

The expectation value of the length of the return series will be

$$\sum_{i=n/7}^{7n} i \frac{7n}{48i^2} = \frac{7\ln(7)}{24} n \, , \tag{3.38}$$

so I shall define q_1 as $\frac{7\ln(7)}{24} \approx 0,5676$.

Let X_1 be the subset corresponding to the trap (the thickened arcs in Figure 21), and

$$f_1(x) = \begin{cases} 1 & \text{if } x \in X_1; \\ 0 & \text{if not.} \end{cases} \tag{3.39}$$

Analogously to Equation (3.34), the correlation of the indicator function of the trap can be approximated by

$$C_{f_1}(n) \approx \frac{\mu(Y_n)}{\mu(X_1)} \, , \tag{3.40}$$

where Y_n is a corridor of the trap of case 3 (see Section 3.4.1).

I will now determine $\mu(Y_n)$ in the exact same way as in Section 3.4.1:

$$\mu(Y_n) = \sum_{k=k_{11}}^{\infty} \sum_{m=max[0,\lceil n - \frac{q_1}{1-q_1} k \rceil]}^{k} \mu(M_3^k) = \sum_{k=k_{11}}^{k_{12}} \sum_{m=\lceil n - \frac{q_1}{1-q_1} k \rceil}^{k} \mu(M_3^k) + \sum_{k=k_{12}}^{\infty} \sum_{m=0}^{k} \mu(M_3^k) \, , \tag{3.41}$$

where $k_{11} = n(1-q_1)$ and $k_{12} = \frac{1-q_1}{q_1} n$ are the intersection points of the appropriate bounding lines (similarly to Figure 25). This yields

$$\mu(Y_n) \approx \sum_{k=(1-q_1)n}^{\frac{1-q_1}{q_1}n} \left(\frac{k}{1-q_1} - n\right) \mu(M_3^k) + \sum_{k=\frac{1-q_1}{q_1}n}^{\infty} k\mu(M_3^k) \approx$$

$$\sum_{k=(1-q_1)n}^{\frac{1-q_1}{q_1}n} \left(\frac{k}{1-q_1} - n\right) \frac{8R\Phi^2}{k^3} + \sum_{k=\frac{1-q_1}{q_1}n}^{\infty} k\frac{8R\Phi^2}{k^3} = \frac{4R\Phi^2(1+q_1)}{1-q_1}\frac{1}{n} \,. \tag{3.42}$$

Since $\mu(X_1) = 8\Phi R$, the correlation function will be

$$C_{f_1}(n) \approx \frac{4R\Phi^2(1+q_1)}{8\Phi R(1-q_1)}\frac{1}{n} = \frac{\Phi(1+q_1)}{2(1-q_1)}\frac{1}{n} \approx 1,813\frac{\Phi}{n} \,. \tag{3.43}$$

4 Numerical simulations

4.1 The programs

I have written two programs for measuring the decay rate of the correlations corresponding to various easily determinable functions, and the Lyapunov exponent in certain billiards.

The parameters of the billiard can be given in an input file in each program:

- n: the number of steps within one trajectory
- N: the number of trajectories calculated (or components in the sample)
- r, R, d: the geometrical parameters of the squash: the radii of the arcs and the distance between their centers.

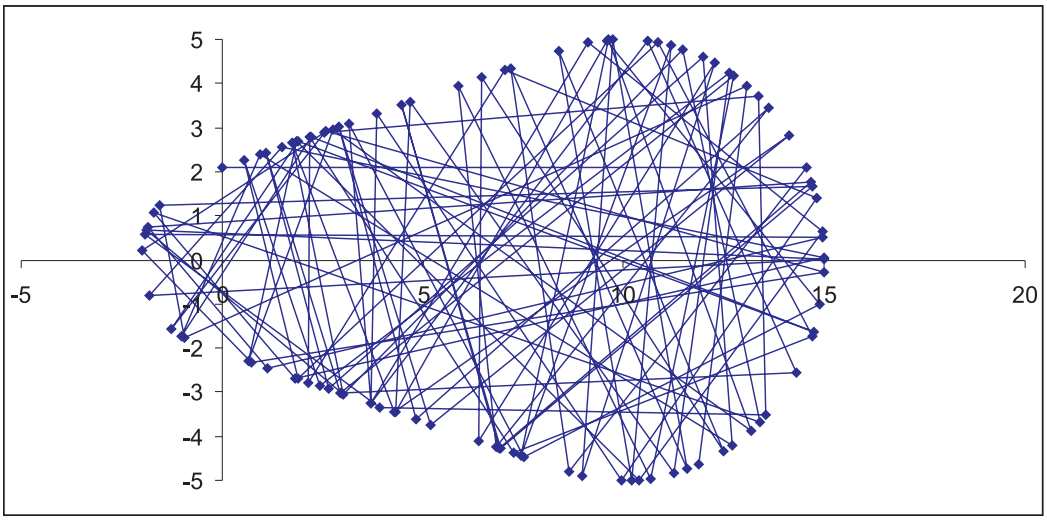

Figure 28: *A simulated trajectory in a squash with* $n = 100$, $r = 2$, $R = 5$, $d = 10$.

The main parts of the programs:

1. The input parameters are read, global constants defined.
2. For every trajectory (of N), an initial state is picked out randomly according to the invariant measure (see Section 2.2). This is done by the function "randstart", (See the program appended). The random number generator we have used is the

so-called Mersenne-twister.
(See [18] or the site http://www.math.sci.hiroshima-u.ac.jp/~m-mat/eindex.html for further details.)

3. Using the given input parameters and the randomly selected initial conditions, the trajectories are calculated up to n collisions.

4. The observed functions are calculated and printed in the output file.

4.2 Some obstacles of numerical experiments

4.2.1 Finite size effects

When we determine any property numerically, we have to avoid trajectories that are periodic, not general or "bad" in any other way. In a mixing system, the total measure of these orbits adds up to zero, but in a numeric simulation, one has to be aware of the bounds set up by the finiteness of computations.

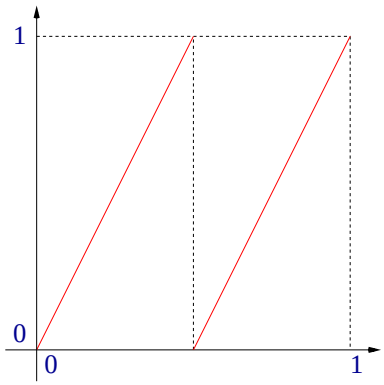

Figure 29: *The map* $f(x) = \{2x\}$

As an example of such phenomenon, consider the following mapping: Let S be the unit interval, and $f : S \to S$ be the function $f(x) = \{2x\}$ (see Figure 29).

Since the computer works on a 32-bit base, any random initial x will eventually (at most in 32 steps) be mapped into the number 0. Because of this, there is no point in trying to run simulations for over 32 steps, for it will not give any useful information.

In my simulations, I did not seem to run into such problems in any apparent way. As far as the number of iterations I have made in any of the programs, I have not noticed any periodicity. And even if a few of the trajectories calculated in one run misbehave, it does not effect the results in any significant way, for our results are gained by averaging.

4.2.2 Long computational time

The largest difficulties I had to face were due to the length of the computational time needed in order to produce near-accurate results. Running one program up to only $n = 500$ steps with a sample size of $N = 10^8$ takes over three hours on the computer used. This means that since the program takes $\mathcal{O}(n \cdot N)$ units of time, I was not able to raise the number of steps with whole orders of magnitude without decreasing N, which was impossible because of statistical reasons described in Section 4.2.3.

It would have been important to be able to perform many steps in cases where the lower order effects still showed up and distorted the observed decay. Also greater samples would have been needed at examining fast decaying functions to avoid fluctuations described in Section 4.2.3.

4.2.3 Fluctuations caused by the deviation

In many cases another problem appeared because of the deviation caused by the finite size of the sample. When the size of the sample is N, the order of the standard deviation from the actual correlation is $\mathcal{O}(1/\sqrt{N})$. Once the correlation has fallen below this limit, the data becomes unusable, as it is demonstrated in Figure 30. To decrease the deviation by one order of magnitude, N has to be increased by two, which results in 100 times longer computational time.

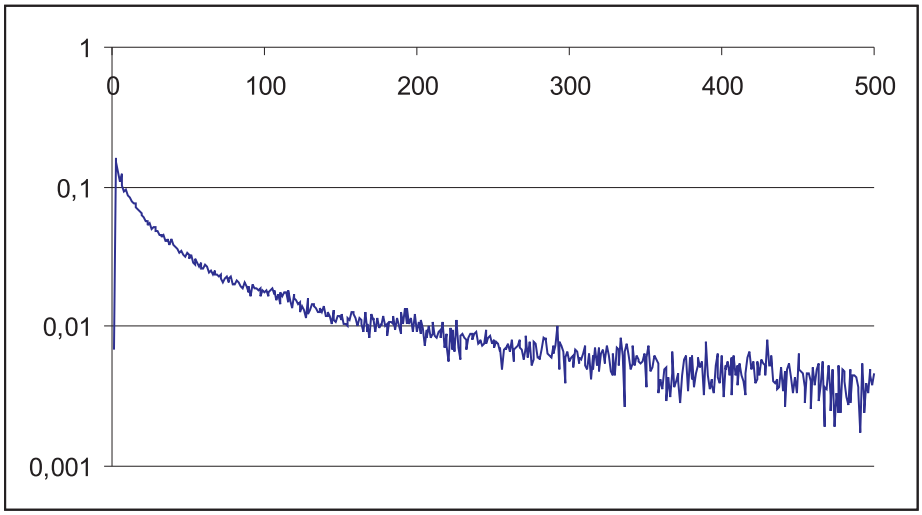

Figure 30: *The decay of the correlation function on a one-log scale in the squash* $r = 2$, $R = 5$, $d = 10$, *with the sample size of* 10^6 *and the indicator function of the straight lines. The one-log scale is used to show that the error is large compared to the correlation, once the latter has decayed enough. It can be very clearly seen that the error is about* $\frac{c}{10^3}$.

As mentioned in Section 4.2.2, I did not have the possibility to execute programs with long runtime (since I definitely had to keep N big, this forced an upper bound on n), so I had to restrict the simulations to certain squashes and stadiums, in which the decay was slow enough to stay above the range of the deviation in the first n steps. Of course, I had to try to simulate many billiards before knowing which would give useful information.

4.2.4 Too small observables, extreme cases

In some cases (for example, when using the indicator function of the trap of case 3 in a squash with either too small or too large Φ or in a stadium with small or large L/r), where some expected values become too small, convergence of the average of simulated numbers to this expected value becomes unmeasurable. A good example of such phenomenon is the following case:

Consider a squash with the parameters $r = 1$, $R = 101$, $d = 100,01$. This gives us a squash with $\Phi = 1,55665$, which is almost $\pi/2$, so it is very much like a circle. The simulated correlation "decay" of the indicator function of the arcs can be seen in Figure 31.

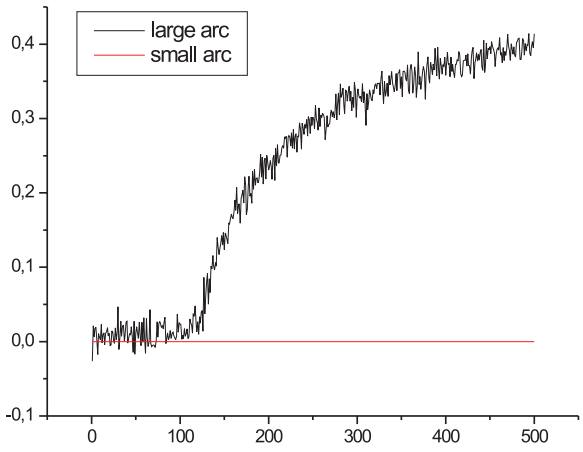

Figure 31: *The "decay" of the correlation functions corresponding to the indicator functions of the given domains for* $r = 1$, $R = 101$, $d = 100,01$.

Let us take a closer look at the raw output of the calculation: Since the probability measure of the small arc is $0,000045$, the probability that a trajectory starts from the little arc and returns there in the k-th step is about $(4,5 \cdot 10^{-5})^2$ when k is large. Because of this, the expected value of the number of such trajectories among the 10^8 is about $(4,5 \cdot 10^{-5})^2 \cdot 10^8 = 0,2025$ which is almost zero. What we see is that for every

$k \leq n$, the number of trajectories out of the 10^8 for which this happens in the k-th step is actually zero. This results in the constant negative (it is a little below 0 which can't be seen on the Figure 31) correlation function of the small arc and also effects the other observables as well (see Section 4.4).

What we see in Figure 31 corresponding to the large arc is of course not a decay. However the following things could produce such phenomenon:

One possible explanation could be that according to [19], the correlation decay corresponding to the speed coordinates of the particle in dispersing billiards measured in continuous time follows a semi-periodic structure with a period that stays about constant in time. If I had done simulations in continuous time, I would probably have seen something similar in our non-dispersing billiards also. Of course not for the same indicator functions I used, but some extensions of them that have appropriate nonzero integrals.

When measuring the correlation function in the moments of the collisions only, we rescale the time of the decay. By doing this, it is possible, that (as in our almost-circle) we only take a look at the continuous time decay with a time shift that is about the time of the free flight across the billiard. If the length of the shift is close to some multiples of the original period, one can experience such non-decay at first sight (see Figure 32). However if this is right, and I would have the resources to simulate much longer trajectories, after a while one would definitely have to see that the function begins to decay.

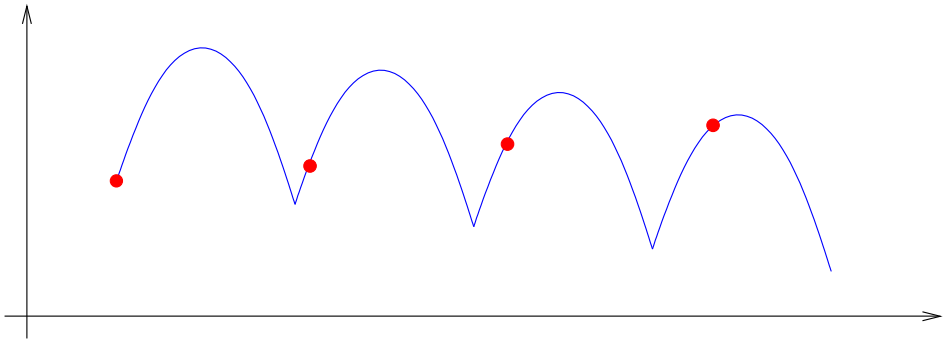

Figure 32: *Even if a function is decaying in continuous time, we may find discrete moments where sampling gives a non-decaying function for some time. Of course, when continuing the observation, even the discrete sample would begin to decay.*

This however not the only possible explanation. It could be that the effects of the almost-integrability of trajectories simply do not allow the correlation to decay in such a short time, since the system resembles an integrable one and also behaves like it at first sight.

4.3 The Lyapunov-exponent

One way to study the chaotic behavior of a system is by looking at its Lyapunov exponent [14]. This value characterizes the separation of originally close phase space orbits, or in other words it expresses the unpredictability of the system caused by the high sensitivity to the initial setup.

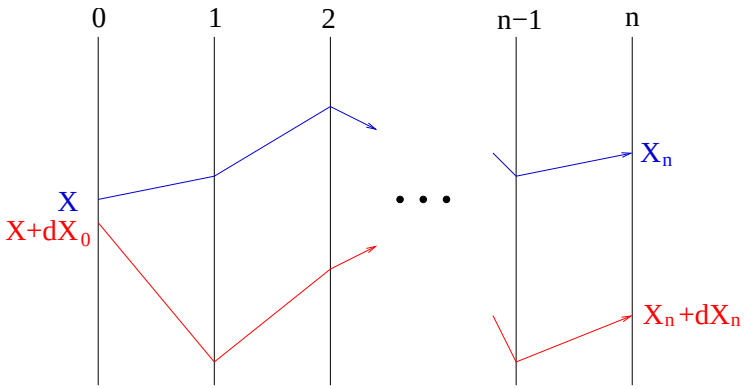

Figure 33: *The change in* $\mathrm{d}x$

If the original separation from the state x was $|\mathrm{d}x_0|$ (see Figure 33), where $\mathrm{d}x_0$ is a typical perturbation, and this separation becomes $|\mathrm{d}x_n|$ at time n, then if the formula

$$|\mathrm{d}x_n(x)| = |\mathrm{d}x_0|e^{\lambda(x)n} \tag{4.1}$$

holds in the limit $n \to \infty$, the number λ is called the Lyapunov exponent in state x. In order to get an exponent that characterizes (μ-almost every point of) the whole system, ergodicity is needed, which in our case is given.

The ratio $\frac{\mathrm{d}x_n}{\mathrm{d}x_0}$ is known as the Jacobian matrix $\mathbf{J}_n$ of the orbit. If the largest eigenvalue of $\mathbf{J}_n$ is Λ_n, then the Lyapunov exponent can be calculated as follows:

$$\lambda = \lim_{n\to\infty} \frac{\ln|\Lambda_n|}{n} \,. \tag{4.2}$$

This exponent can tell us much of the reliability of computer simulations. Because of the finiteness of computational possibilities, the accuracy of the computer is only true up to a number of digits. After many steps, the error caused by this rounding will grow high in a system with a large λ. This means that the trajectory corresponding to some given initial conditions will be very different from the trajectory simulated.

This fact will hopefully not effect our observed amounts (i.e. the correlation decay rate), because there exists another trajectory that is relatively close to ours:
Let us define the following: A sequence of points $(x_i)_{i\in\mathbb{Z}}$ is an *ε-pseudo orbit* of T if $\forall i \in \mathbb{Z}$, $d(T(x_i), x_{i+1}) < \varepsilon$.

Lemma 4.1 ***Shadowing lemma:*** *Let Λ be a compact, invariant, hyperbolic set for a C^2-smooth map T. For all $\delta > 0$ sufficiently small there exists $\varepsilon > 0$ and a neighborhood U of Λ such that each ε-pseudo orbit (x_i) in U is δ- shadowed by a unique real orbit. In other words there exists a unique $y \in \Lambda$ such that $d(T^i(y), x_i) < \delta \ \forall i \in \mathbb{Z}$.*

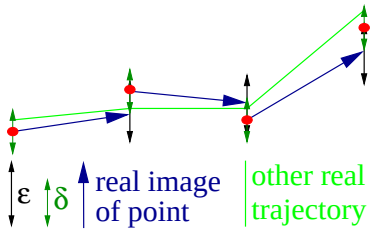

Figure 34: *Shadowing lemma: the (red) pseudo orbit, and a real trajectory.*

The shadowing theory has only been dealt with so far in uniformly hyperbolic cases, but it can be conjectured to hold in our case also, since the return map is uniformly hyperbolic. If it holds, it can make sure that the simulated results are close to the real amounts, for I take the averages of certain functions calculated, so being a little "off" probably has no effect.

I must also mention that even if shadowing does hold, simulating could in some cases result in destroying the invariant measure, if the pseudo map does not leave it invariant. (For example, the map $f(x) = \{2x\}$ mentioned in Section 4.2.1 leaves the Lebesgue measure invariant, but the pseudo map does not: its invariant measure has to be concentrated on the number 0. All pseudo-orbits are shadowed by trajectories running into 0.) This will of course result in false data. However, there are ways to evade such difficulties, for example by adding a small random error to the image in each step.

See also [9, 15] on the topic of shadowing.

4.3.1 The lyap.c program

The program I have written in order to get a hint of the Lyapunov exponent in the squash billiard works the following way:

In order to calculate the derivative of the k-th iterate of T for some $k < n$, we follow a trajectory and calculate the derivative matrix at the consecutive points. These matrices are then multiplied according to the chain rule:

$$DT^k(x) = DT(T^{k-1}(x)) \dots DT(T(x))DT(x) \tag{4.3}$$

These manipulations are performed in the four dimensional coordinate system, thus at the end we project it to the two dimensional subspace that is relevant for us

at x. That is, we calculate the perturbation in position parallel to the tangent of the boundary, and in velocity, perpendicular to the speed vector at x. What results is a 2×2 matrix, for which the eigenvalue of larger absolute value (Λ_k) is to be calculated. This is repeated N times, then the outcomes are averaged (as in Section 4.4, Equation (4.4)).

Once this was done, the exponent can be estimated when (k,Λ_k) is plotted on a one-log scale as the slope of the almost-linear curve (Figure 35).

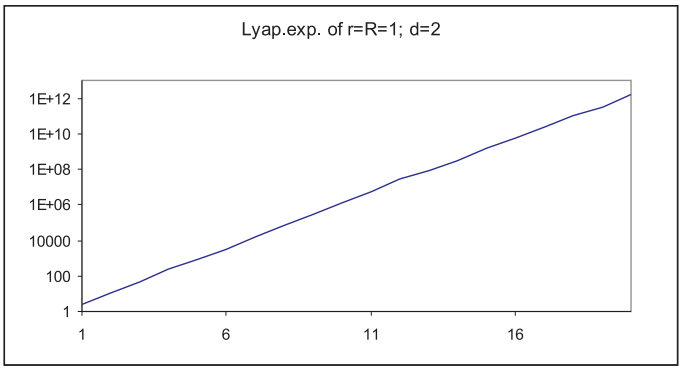

Figure 35: *The estimated Lyapunov exponent on a one-log scale in the stadium with the parameters* $r = 1$, $d = 2$. *The estimated gradient:* $\lambda \approx 1,44$

The λ achieved here is of course a function of the size of the stadium and of the fact that I have only simulated in discrete time. If I simulate for a squash twice as big, the exponent will change, for the small differences caused by perturbations will have twice as much free flight to grow and the local curvature will also change.

For more information on the Lyapunov exponents of billiards, see [10, 11, 14].

4.4 The correlation decay through simulations

Let us fix n, and take N i.i.d. random variables: $f(x_i)f(T^n(x_i))$ for x_i calculated according to μ', $i = 1 \dots N$. Then by the law of large numbers,

$$\frac{1}{N} \sum_i f(x_i) f(T^n(x_i)) \to \int f(x) f(T^n(x)) \mathrm{d}\mu'(x) \ . \tag{4.4}$$

I will thus calculate N times the functions of which we need the expectation value, then take the averages of the outcome for each step of the n.

4.4.1 The stadium and the indicator function of the trap

Now I will try to verify the heuristical deduction made in Section 3.4.1 numerically, so I will restrict to the indicator function of the trap of case 1.

Some results of the execution of the program that measures the decay of the correlation function in some stadiums can be seen in Figure 36. The gradient is about -1 at the end of the curves on the log-log scale, so the decay of $\mathcal{O}(\frac{1}{n})$ can be measured here nicely. What can't be observed here is the constant that the $\frac{1}{n}$ is multiplied by. However, this constant can change a lot when the gradient only changes a little, so this is not surprising.

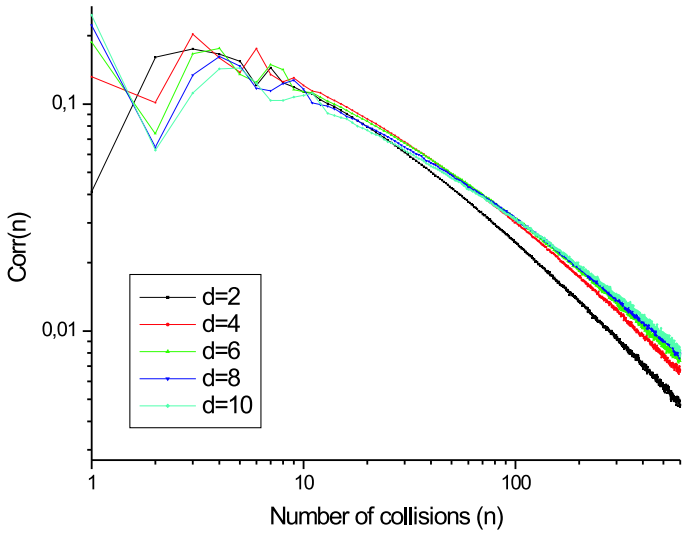

Figure 36: *The simulated decay of correlations in different stadiums:* $r = 1$, d *varying. The slope of the curves at the end is a little greater than* -1.

My conjecture was $C_{f_0}(n) = \frac{a}{n} + o(\frac{1}{n})$. To find the best possible value for a, a log-log scale was not appropriate. Instead, I have tried plotting the data $nC_{f_0}(n)$, so when n is large enough, it will tend to the constant a. The results can be seen in Figure 37, where it became clear, that the number of steps I am able to simulate are not even nearly enough, for the curves seen are far from being constant even when n is close to 600.

The curve corresponding to $d = 2$ was the closest to being constant, but as one can see, it is only around 3 at most instead of the $2 \cdot 2,59$ I have calculated in Section 3.4.1.

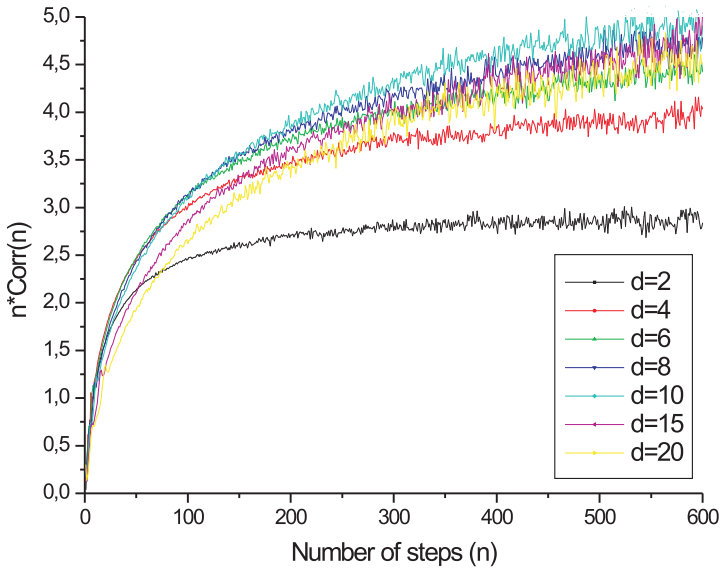

Figure 37: $nC_{f_0}(n)$ *in different stadiums:* $r = 1$, d *varying.*

In order to see how far the simulated curve is from the one it has to tend to as $n \to \infty$ (according to my calculations), I have plotted both in Figure 38. It does not seem to be impossible that the simulated curve will eventually lean into the line, though that is not what one would think of right away.

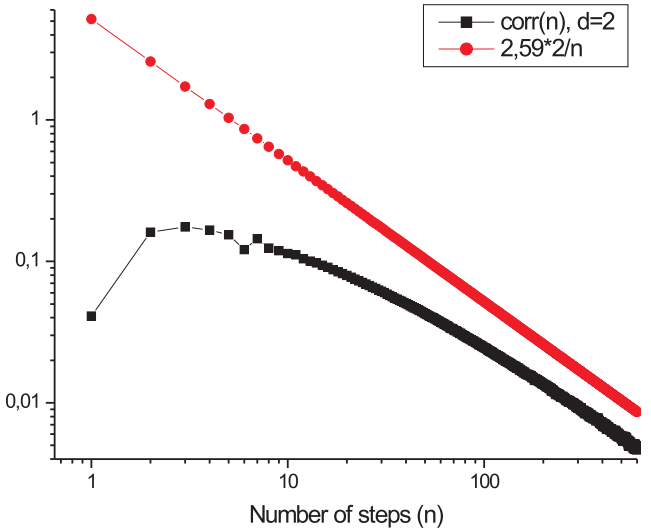

Figure 38: *The difference between the simulated decay and the first order calculations of the rate.*

Because of reasons described in Section 4.2.4, it is also not too surprising that the correlation functions do not show monotone dependence to the parameter L (which equals to d) in the first "few" steps. When d is large compared to r, what we have is an almost-tunnel with very little "dispersing" surfaces. Also, as I have said in Section

4.2.2, I did not have the opportunity to simulate long trajectories, and it seems here that the lower order effects are inevitably visible.

4.4.2 The squash and the indicator function of the trap

The outcome of some of the simulations can be seen in Figure 39. The picture shows decays with the initial fluctuations growing as Φ is increased. One can also immediately see that the slope of the curves near the end (but before the fluctuations caused by the variance begin) is about -1.

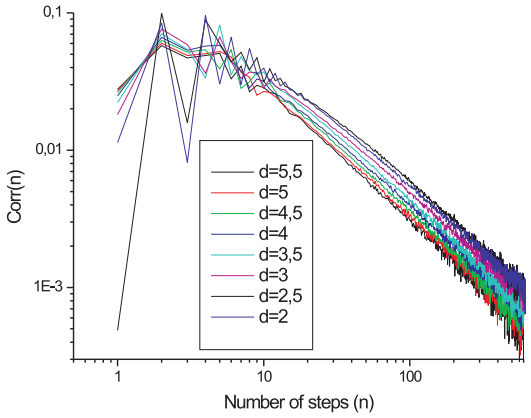

Figure 39: *Correlation decay in squashes with $r = 1$, $R = 2$, d varying.*

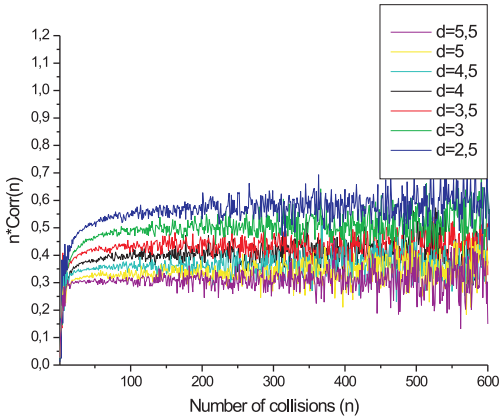

Figure 40: *The product of n and $C_{f_1}(n)$ in various squashes with $r = 1$, $R = 2$, d varying.*

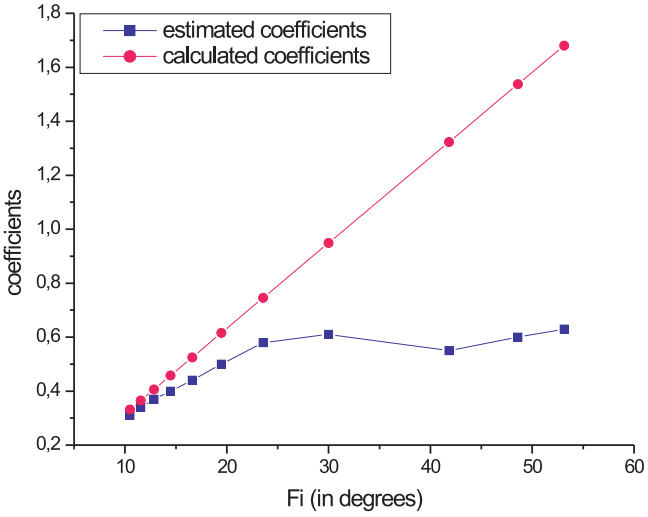

Figure 41: *The difference between the estimated and the heuristically calculated coefficients of $\frac{1}{n}$.*

Figure 41 above shows the calculated and the estimated coefficients in squashes with the parameters $r = 1$, $R = 2$, d varying. As one can see, the coefficients of $1/n$ again differ from the simulated value in most cases. The figure shows that lower order effects are present in a stronger way when Φ is large (see Section 4.2.4), for I only got coefficients close to the expected ones when Φ was around 10 degrees. The lower order terms seem to decay much faster when Φ is not large, which means that their coefficients are probably smaller.

The difference between the estimated and the calculated lines in one of the above examples can be seen on Figure 42:

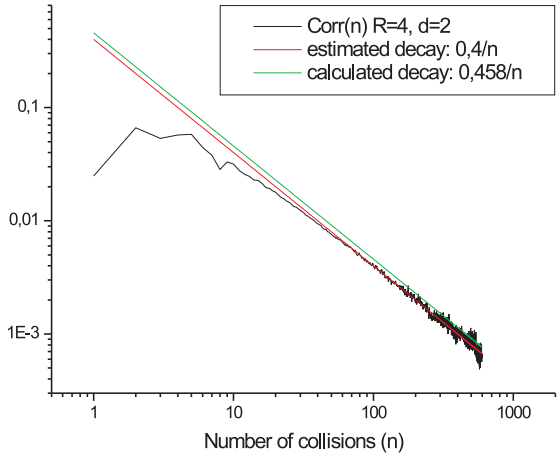

Figure 42: *The distance between the estimated and the calculated coefficients. The parameters are* $r = 1$, $R = 2$, $d = 4$, *and* $\Phi = 14,5°$.

As one can see, the calculated curve is not very far from the line fitted on the simulated data, even though it is not the closest to our calculations.

5 Summary

In my thesis, I have selected a specific family of billiards in which I studied the rate of the decay of correlations for various functions. Since the Bunimovich stadium has already been partially studied in this respect, I have chosen to widen the subject of the study to the squash-shaped billiards.

These billiards consist of two arcs with the radii r and R whose centers are placed at a distance of d and connected with their common outer tangent. The lines that connect the arcs are L long and disclose the angle Φ with the segment connecting the centers of the circles.

As it is known, the rate of the decay is slower than exponential in both cases. This is a result of the presence of long segments of integrable motion. I have given a first order estimate for the measure of the subsets (the traps) that are responsible for such regular trajectories: In the stadium, the measure of the subset starting from which the trajectories bounce n times between the two parallel lines is $\frac{2d^2}{rn^3}$, and in the squash, the measure of the starting points of trajectories that complete n consecutive collisions across the larger arc near its diameter is $\frac{8R\Phi^2}{n^3}$.

Based upon this, I gave a first order approximation for the rate of the decay of correlations corresponding to the indicator functions of the traps: In the stadium, this value is about $2,59\frac{d}{rn}$ and in the squash, $1,813\frac{\Phi}{n}$.

I have also tried to verify the calculated decay rates through simulations. This attempt was not always successful, however I have built up conjectures that might explain the reasons why. These studies have provided further evidence that the dynamical behavior of chaotic billiards is a very subtle issue, simulating which requires special care. Among others, it is worth mentioning a good choice of the sample size versus the number of simulated collisions (the parameters N and n); a suitable selection of the geometric parameters (extremely long stadia and almost-circle squashes typically produce strange simulation results) and the careful evaluation of data (simultaneous use of linear and log-log scaled plots).

Many questions remained open, mostly in the topic of the simulations. Based on my above sketched experiences, I would like to continue these numerical studies in the future. For example, it would be interesting to try to approximate the second order of the decays, or to proceed on to semi-dispersing or even higher dimensional billiards. Also it would be nice to simulate the exact size-dependence of the Lyapunov exponent.

Acknowledgements

First of all, I would like to express my gratitude to Imre Péter Tóth for his help in programming and running the simulations, for the technical discussions about evaluating the results and for his guidance and help throughout my thesis-writing period. I thank Péter Bálint for his helpful comments concerning the mathematical contents, for his support and assistance in writing the thesis, but also for his great efforts to keep me inspired. I am also very grateful to András Vetier for his enthusiastic supervision: he provided encouragement and good advice whenever I needed it.

References

[1] B. J. Alder, T. E. Wainwright, *Decay of the Velocity Autocorrelation Function*, Phys. Rev. A 1, 18-21, 1970

[2] P. Bálint, S. Gouezel, *Limit theorems in the stadium billiard*, oai:arXiv.org:math/0502453, 2005

[3] L. A. Bunimovich, *On billiards close to dispersing*, Math. USSR Sbornik, 23, 45-67, 1974

[4] L. A. Bunimovich, *On the ergodic properties of nowhere dispersing billiards*, Comm. Math. Phys. 65, 295-312, 1979

[5] L. A. Bunimovich, *On absolutely focusing mirrors*, Lect. Notes Math., 1514, 62-82, Springer, New York, 1990

[6] L. A. Bunimovich, and Ya. G. Sinai, *Statistical properties of Lorenty gaz with periodic configuration of scatterers*, Comm. Math. Phys. 78, 479-497, 1981

[7] N. Chernov, L.-S. Young, *Decay of correlations for Lorentz gases and hard balls*, in: Hard Ball Systems and the Lorentz Gas, D. Szasz, ed., Encyclopaedia of Mathematical Sciences 101, pp. 89-120, Springer, 2000

[8] N. Chernov, H.K. Zhang, *Billiards with polynomial mixing rates*, Nonlinearity 18, 1527, 2005

[9] Clark Robinson, *Dynamical systems : stability, symbolic dynamics, and chaos*, CRC Press, Inc., 1995

[10] P. Dahlqvist, *Decay of correlations, Lyapunov exponents and anomalous diffusion in the Sinai billiard*, Nonlinearity, 8, 11, 1995.

[11] Ch. Dellago, H. A. Posch, *Lyapunov exponents of systems with elastic hard collisions*, Phys. Rev. E 52, 2401, 1995

[12] M. Denker, *The central limit theorem for dynamical systems*, Dyn. Syst. Ergod. Th. Banach Center Publ., 23, PWN–Polish Sci. Publ., Warsaw, 1989

[13] Donnay V., *Using integrability to produce chaos: billiards with positive entropy*, Comm. Math. Phys. 141, 225-257, 1991

[14] J. L. Hansen, *Lyapunov exponents for the stadium billiard*, Phys. Rev. Lett. 52, 2388, 1995

[15] Katok A., Hasselblatt B, *Introduction to the Modern Theory of Dynamical Systems*, Encyclopedia of Mathematics and its Applications 54, Cambridge University Press, 1995

[16] Markarian, R., *Billiards with Pesin region of measure one*, Comm. Math. Phys. 118, 87-97, 1988

[17] Markarian, R., *Billiards with polynomial decay of correlations*, ETDS 24, 177, 2004

[18] M. Matsumoto and T. Nishimura, *Mersenne Twister: a 623-dimensionally equidistributed uniform pseudorandom number generator*, ACM Transactions on Modeling and Computer Simulation 8, 3-30, 1998

[19] Pedro L. Garrido, Giovanni Gallavotti: *Billiards correlation functions*, Journal of Statistical Physics, 76, 549-586, 1994

[20] Sinai, Ya.: *Dynamical systems with elastic reflections. Ergodic properties of dispersing billiards*, Russian Mathematical Surveys, 25, 137-189, 1970

[21] Vivaldi,F., Casati, G. and Guarneri, I., *Origin of long-time tails in strongly chaotic systems*, Phys. Rev. Lett. 51, 727-730, 1983

[22] Wojtkowski, M. P., *Principles for the design of billiards with nonvanishing Lyapunov exponents*, Commun. Math. Phys. 105, 391-414, 1986

[23] L.-S. Young, *Statistical properties of dynamical systems with some hyperbolicity*, Ann. of Math. 147(3), 585-650, 1998

Appendix

Software

- The figures inserted were made using Xfig (http://www.xfig.org)
- The results of the executed programs were processed by
  - QtiPlot (http://soft.proindependent.com/qtiplot.html)
  - Origin (http://www.originlab.com)
  - Excel (http://www.microsoft.com)
- Typesetting by LaTeX (http://www.tug.org, http://www.miktex.org)

The program squash.c

```
1  #include <stdlib.h>
2  #include <stdio.h>
3  #include <math.h>
4  #include "mt.h"  /* The Mersenne Twister random number generator */
5
6  /* names of the curves */
7  const char LEFTARC=1;
8  const char TOPLINE=2;
9  const char RIGHTARC=3;
10 const char BOTTOMLINE=4;
11
12 /* global constants - only defined once */
13 int n,Nf;
14 double r,R,d,l,a,b,A,B,nx,ny,c,circumference,smallarc,largearc,fi;   /* geometric data */
15 double Rmr,r2,r2inv,R2,R2inv,nx2,ny2,rinv, Rinv;
16                         /* auxiliary constants for the computations */
17
18
19
20 /* the 5 coordinates of the phase space */
21 char piece;
22 double x,y,vx,vy;
23
24 /* auxiliary variables for the simulation */
25 double t,coll,VxX,vxb,vya,vxB,vyA,VN,XV,Vabs;
26
27 /* else */
28 int k1,k2;
29
30
31 /* Random start */
32 double sinangle, cosangle; /* initial angle of incidence */
33 void randstart(double *px,double *py,double *pvx,double *pvy,char *ppiece){
34         double arclength=0; /* this will be uniformly distributed */
35
36         double delta,sindelta,cosdelta;
```

```
37
38          arclength=genrand_real1();
39          arclength=arclength*circumference;
40          sinangle=genrand_real1();
41          sinangle=2*sinangle-1;
42          cosangle=sqrt(1-sinangle*sinangle);
43
44          if(arclength<=l){
45                  (*px)=a+ny*arclength;
46                  (*py)=-b+nx*arclength;
47                  (*pvx)=-nx*cosangle+ny*sinangle; /* =cos(PI/2-angle-Fi) */
48                  (*pvy)=ny*cosangle+sinangle*nx; /*=sin(PI/2-angle-Fi)*/
49                  (*ppiece)=BOTTOMLINE;
50          }
51          else if(arclength>l && arclength<=l+largearc){
52                  arclength=arclength-l;
53                  delta=arclength/R-fi;
54                  sindelta=sin(delta);
55                  cosdelta=cos(delta);
56                  (*px)=d+R*sindelta;
57                  (*py)=-R*cosdelta;
58                  (*pvx)=-cosangle*sindelta-sinangle*cosdelta;/*=cos(angle+delta+M_PI_2)*/
59                  (*pvy)=-sinangle*sindelta+cosangle*cosdelta;/*=sin(angle+delta+M_PI_2)*/
60                  (*ppiece)=RIGHTARC;
61          }
62          else if(arclength>l+largearc && arclength<=2*l+largearc){
63                  arclength=arclength-l-largearc;
64                  (*px)=A-arclength*ny;
65                  (*py)=B+arclength*nx;
66                  (*pvx)=-cosangle*nx+sinangle*ny;/*=cos(Fi-M_PI_2+angle)*/
67                  (*pvy)=-sinangle*nx-cosangle*ny;/*=sin(Fi-M_PI_2+angle)*/
68                  (*ppiece)=TOPLINE;
69          }
70          else if(arclength>2*l+largearc && arclength<= circumference){
71                  arclength=arclength-2*l-largearc;
72                  delta=arclength/r+fi;
73                  sindelta=sin(delta);
74                  cosdelta=cos(delta);
75                  (*px)=-r*sindelta;
76                  (*py)=r*cosdelta;
77                  (*pvx)=cosangle*sindelta+sinangle*cosdelta;/*=cos(angle-M_PI_2+delta)*/
78                  (*pvy)=sinangle*sindelta-cosangle*cosdelta;/*=sin(angle-M_PI_2+delta)*/
79                  (*ppiece)=LEFTARC;
80          }
81          else {
82                  printf(" Trouble with the random start!!! \n");
83          }
84  }
85
86  double Sinrefl(double lx,double ly,double lvx,double lvy,char lpiece){
87          double sinrefl;
88          switch(lpiece) {
89                  case 1:/*LEFTARC*/
90                          sinrefl=rinv*(lx*lvy-ly*lvx);
91                  case 2:/*TOPLINE*/
92                          sinrefl=-ny*lvx+nx*lvy;
93                  case 3:/*RIGHTARC*/
```

```
                        sinrefl=Rinv*((lx-d)*lvy-ly*lvx);
                case 4:/*BOTTOMARC*/
                        sinrefl=ny*lvx+nx*lvy;
        }
        return sinrefl;
}
int F(double Piece){
        if(Piece==TOPLINE||Piece==BOTTOMLINE)return 1;
        else return 0;
}

double S1[1000];int S2[1000];

main(int argc, char *argv[]){

/* Reading input data */

        FILE *input,*output;  /* input and output files */

        if (argc!=3) {
                printf("use of program:\n a.out <parameter file>"
               " <output file>\n");
                return -1;
        }

        input=fopen(argv[1],"rt");      /* input file opens */

        if (input==NULL) {
                printf ("Bad input file! \n");
                return -1;
        }
        /* reading constants from input */
        double dd;
        fscanf(input,"n %d\nNf %d\nr %le\nR %le\nd %le", &n,&Nf,&r,&R,&dd);
        fclose(input);
        d=dd;

        output=fopen(argv[2],"wt");     /* output file opens */

/* defining global constants */
Rmr=R-r; l=sqrt(d*d-Rmr*Rmr);
a=-r*Rmr/d; b=r*l/d;
A=d-R*Rmr/d; B=R*l/d;
nx=(b-B)/l; ny=(A-a)/l; c=r;
fprintf(output,"n=%d  Nf=%d\n",n,Nf);
fprintf(output,"r=%f  R=%f  d=%f l=%f\n",r,R,d,l);
fprintf(output,"a=%f  b=%f  A=%f  B=%f\n",a,b,A,B);
fprintf(output,"N\tSspeed(n)\tCorr\tSegy(n)\tCorr(n)\n",a,b,A,B);
//printf("nx=%f  ny=%f  c=%f\n",nx,ny,c);

fi=asin(-nx); /*the angle of the straight lines with the horizontal line*/
smallarc=r*(M_PI-2*fi);
largearc=R*(M_PI+2*fi);
circumference=2*l+smallarc+largearc;

double p;
p=2*l/circumference;
```

```
151
152  r2=r*r; rinv=1/r; Rinv=1/R; r2inv=rinv*rinv; R2=R*R; R2inv=Rinv*Rinv;
153  nx2=2*nx; ny2=2*ny;
154
155
156
157  /* generating the initial conditions: */
158
159  unsigned long init[4]={0x123, 0x234, 0x345, 0x456}, length=4;
160  init_by_array(init, length);    /* needed for mt.h */
161
162
163  /* the cycle begins */
164  for(k1=0; k1<=n; k1++){
165          S1[k1]=0;
166  }
167
168  /* one trajectory */
169  for(k2=1;k2<=Nf;k2++){
170
171  if(Nf/2<k2 && k2<=Nf/2+1){
172          printf("Half way though! r=%f R=%f d=%f\n",r,R,d);
173  }
174
175  randstart(&x,&y,&vx,&vy,&piece);
176  S1[0]=S1[0]+Sinrefl(x,y,vx,vy,piece)*sinangle;
177  S2[0]=S2[0]+F(piece);
178
179
180  /* before the first step: */
181  if(piece==LEFTARC) {t=-2*(x*vx+y*vy); coll=t*r2inv;}
182  if(piece==RIGHTARC) {x-=d; t=-2*(x*vx+y*vy); coll=t*R2inv; x+=d;}
183
184  for(k1=1;k1<=n;k1++){
185
186  /* one step of a trajectory: */
187  VxX=vx*y-vy*x; vxb=vx*b; vya=vy*a; vxB=vx*B; vyA=vy*A;
188  switch(piece) {
189          case 1: /* LEFTARC */
190                  if(VxX<-vxb-vya){
191                          /* piece=LEFTARC; */
192                          /* XV=x*vx+y*vy; t=sqrt(XV*XV+r2-x*x-y*y)-XV; */
193                          x+=t*vx;
194                          y+=t*vy;
195                          /* t=2*(x*vx+y*vy); coll=t*r2inv; */
196                          vx-=coll*x;
197                          vy-=coll*y;
198                          }
199                  else if(VxX<=-vxB-vyA){
200                          piece=BOTTOMLINE;
201                          VN=vx*nx-vy*ny;
202                          t=(c-x*nx+y*ny)/VN;
203                          x+=t*vx;
204                          y+=t*vy;
205                          vx-=VN*nx2;
206                          vy+=VN*ny2;
207                          }
```

```
208                 else if(VxX<vxB-vyA){
209                         piece=RIGHTARC;
210                         x-=d;
211                         XV=x*vx+y*vy; t=sqrt(XV*XV+R2-x*x-y*y)-XV;
212                         x+=t*vx;
213                         y+=t*vy;
214                         t=2*(x*vx+y*vy); coll=t*R2inv;
215                         vx-=coll*x;
216                         vy-=coll*y;
217                         x+=d;
218                         }
219                 else if(VxX<=vxb-vya){
220                         piece=TOPLINE;
221                         VN=vx*nx+vy*ny;
222                         t=(c-x*nx-y*ny)/VN;
223                         x+=t*vx;
224                         y+=t*vy;
225                         vx-=VN*nx2;
226                         vy-=VN*ny2;
227                         }
228                 else {
229                         /* piece=LEFTARC; */
230                         /* XV=x*vx+y*vy; t=sqrt(XV*XV+r2-x*x-y*y)-XV; */
231                         x+=t*vx;
232                         y+=t*vy;
233                         /* t=2*(x*vx+y*vy); coll=t*r2inv; */
234                         vx-=coll*x;
235                         vy-=coll*y;
236                         }
237                 break;
238         case 3:  /* RIGHTARC */
239                 if(VxX<vxB-vyA){
240                         /* piece=RIGHTARC; */
241                         x-=d;
242                         /* XV=x*vx+y*vy; t=sqrt(XV*XV+R2-x*x-y*y)-XV; */
243                         x+=t*vx;
244                         y+=t*vy;
245                         /* t=2*(x*vx+y*vy); coll=t*R2inv; */
246                         vx-=coll*x;
247                         vy-=coll*y;
248                         x+=d;
249                         }
250                 else if(VxX<=vxb-vya){
251                         piece=TOPLINE;
252                         VN=vx*nx+vy*ny;
253                         t=(c-x*nx-y*ny)/VN;
254                         x+=t*vx;
255                         y+=t*vy;
256                         vx-=VN*nx2;
257                         vy-=VN*ny2;
258                         }
259                 else if(VxX<-vxb-vya){
260                         piece=LEFTARC;
261                         XV=x*vx+y*vy; t=sqrt(XV*XV+r2-x*x-y*y)-XV;
262                         x+=t*vx;
263                         y+=t*vy;
264                         t=2*(x*vx+y*vy); coll=t*r2inv;
```

```
                        vx-=coll*x;
                        vy-=coll*y;
                        }
                else if(VxX<=-vxB-vyA){
                        piece=BOTTOMLINE;
                        VN=vx*nx-vy*ny;
                        t=(c-x*nx+y*ny)/VN;
                        x+=t*vx;
                        y+=t*vy;
                        vx-=VN*nx2;
                        vy+=VN*ny2;
                        }
                else {
                        /* piece=RIGHTARC; */
                        x-=d;
                        /* XV=x*vx+y*vy; t=sqrt(XV*XV+R2-x*x-y*y)-XV; */
                        x+=t*vx;
                        y+=t*vy;
                        /* t=2*(x*vx+y*vy); coll=t*R2inv; */
                        vx-=coll*x;
                        vy-=coll*y;
                        x+=d;
                        }
                break;
        case 2:  /* TOPLINE */
                if(VxX<-vxb-vya){
                        piece=LEFTARC;
                        XV=x*vx+y*vy; t=sqrt(XV*XV+r2-x*x-y*y)-XV;
                        x+=t*vx;
                        y+=t*vy;
                        t=2*(x*vx+y*vy); coll=t*r2inv;
                        vx-=coll*x;
                        vy-=coll*y;
                        }
                else if(VxX<=-vxB-vyA){
                        piece=BOTTOMLINE;
                        VN=vx*nx-vy*ny;
                        t=(c-x*nx+y*ny)/VN;
                        x+=t*vx;
                        y+=t*vy;
                        vx-=VN*nx2;
                        vy+=VN*ny2;
                        }
                else {
                        piece=RIGHTARC;
                        x-=d;
                        XV=x*vx+y*vy; t=sqrt(XV*XV+R2-x*x-y*y)-XV;
                        x+=t*vx;
                        y+=t*vy;
                        t=2*(x*vx+y*vy); coll=t*R2inv;
                        vx-=coll*x;
                        vy-=coll*y;
                        x+=d;
                        }
                break;
        case 4:   /*BOTTOMLINE*/
                if(VxX<vxB-vyA){
```

```
                        piece=RIGHTARC;
                        x-=d;
                        XV=x*vx+y*vy; t=sqrt(XV*XV+R2-x*x-y*y)-XV;
                        x+=t*vx;
                        y+=t*vy;
                        t=2*(x*vx+y*vy); coll=t*R2inv;
                        vx-=coll*x;
                        vy-=coll*y;
                        x+=d;
                        }
                else if(VxX<=vxb-vya){
                        piece=TOPLINE;
                        VN=vx*nx+vy*ny;
                        t=(c-x*nx-y*ny)/VN;
                        x+=t*vx;
                        y+=t*vy;
                        vx-=VN*nx2;
                        vy-=VN*ny2;
                        }
                else {
                        piece=LEFTARC;
                        XV=x*vx+y*vy; t=sqrt(XV*XV+r2-x*x-y*y)-XV;
                        x+=t*vx;
                        y+=t*vy;
                        t=2*(x*vx+y*vy); coll=t*r2inv;
                        vx-=coll*x;
                        vy-=coll*y;
                        }
                break;
        }
Vabs=sqrt(vx*vx+vy*vy); vx/=Vabs; vy/=Vabs;
/* end of step */


S1[k1]+=Sinrefl(x,y,vx,vy,piece)*sinangle;
S2[k1]=S2[k1]+F(piece);

} /* end of trajectory */
} /* end of cycle */

for(k1=0; k1<=n; k1++){
        fprintf(output,"%d\t%f\t%f\t", k1, S1[k1], S1[k1]/Nf);
        fprintf(output,"%d\t%f\n", S2[k1], ((double)S2[k1]/(double)Nf-p)/(1-p));
}

fflush(output);
fclose(output);
return 0;
} /* end of main() */
```